Observing phase changes in real time on ultra-thin Iron oxide surfaces

Harald Wallander

Thesis submitted for the degree of Master of Science
Project duration: 9 months

Supervised by J. Knudsen

LUND
UNIVERSITY

Department of Physics
Division of synchrotron radiation physics

June 20, 2019

Abstract

Studying catalysts under such non-equilibrium conditions is a step towards approaching more realistic reaction conditions for working catalysts. Reactivity during phase changes of ultra-thin FeO_2 films grown on Pt(111) are studied *in situ* with Ambient Pressure X-ray Photo Emission Spectroscopy and Quadrupole Mass Spectrometry, while running the CO oxidation reaction at 160°C and 0.6 mbar. These phase changes are induced by rapidly changing the gas composition of the CO:O_2 feed gas. The composition is changed so that series of 16-second pulses of CO are sent to the sample.

My study showed that CO in the first few pulses is completely oxidised while only the first part of later pules is oxidised. This partial oxidation is explained by gradual CO poisoning of bare Pt(111) patches formed between FeO_2 islands due to dewetting of the FeO_2 film. During CO poisoning, core level shifts indicate a change from FeO_2 trilayer to an oxide film with more FeO bilayer character. The activity of the FeO_2/Pt(111) sample increased gradually and reached higher values than the Pt(111) reference after an incubation time of about one hour.

Contents

Acronyms

APXPS Ambient Pressure X-ray Photo Emission Spectroscopy. i, 6, 10, 14, 17, 27, 33, 35, 36

CUF Coordinatively Unsaturated Ferrous site. 35

LEED Low Energy Electron Diffraction. 2, 4, 5, 12, 13

PMIRAS polarization modulated infrared reflection absorption spectroscopy. 35, 37

QMS Quadrupole Mass Spectrometry. i, 15, 16, 32, 33, 34, 36

STM Scanning Tunnelling Microscopy. 36, 37

TDS Temperature Programmed Desorption. 36

UHV Ultra High Vacuum. 5, 9, 12

XPS X-ray Photo Emission Spectroscopy. 2, 5, 6, 7, 8, 9, 12, 32, 36, 37

1 Introduction

Catalysis is used in a wide range of technological applications that improve our quality of life, with the most well-known example being catalytic converters in auto mobiles. They convert toxic carbon monoxide, nitrous oxides and unburnt fuel from the engine exhaust to harmless water, carbon dioxide and nitrogen. It must be said, that exhaust cleaning is only the tip of the iceberg when it comes to the usefulness of catalysts for humanity: 60% of the world's produced chemicals use catalysis in their synthesis.[1]
To illustrate the impact of this fact let us consider the synthesis of ammonia. Ammonia is produced industrially in the Haber-Bosch process, which relies on catalysis, and is among other things used for the production of artificial fertilisers. The population of Earth went from 1.6 billion in year 1900 to 6 billion in year 2000 mostly thanks to the introduction of artificial fertilisers and roughly nine tenths of the essential amino acids in a human body are made from ammonia that came out of a factory utilising the Haber-Bosch process.[2]
Because of the great use of catalysts in everyday life as well as in industry much effort has been made to understand and explain catalysis. Despite this most catalysts in use today have been discovered by trial and error methods and we are still far from the point where catalysts can be predicted, synthesized and confirmed from a fundamental understanding of catalytic processes.

Over the years several efficient catalysts have been discovered but despite being an old technology and having a long research history, some technical problems with catalysts remain unsolved today. To return to the catalytic converter in cars one problem is that it has a minimum operation temperature, the light-off temperature. As a result, the converter will not work well when the engine is cold. This and reduced fuel efficiency are two main reasons to minimise the number of such "cold starts". Another problem affecting the converter is that the ratio of air and unburned fuel in the exhaust gas must be within certain limits for all pollutants to be converted efficiently.

The catalytic converters used in modern vehicles remove three main pollutants from the exhaust: CO, NO_x and unburned hydrocarbons and are for this reason called 3-way converters. Structurally, 3-way converters consist of a bloc of substrate material with many narrow channels that the exhaust gas can pass through, minimising the distance a gas molecule has to diffuse to reach the surface.[3] The channel walls in the substrate is then coated with an intermediate material called the washcoat, which has nanometre-sized particles of catalysts embedded into it. The purpose of the washcoat is to provide a stable environment for the catalyst and sometimes to provide a way to store oxygen, especially if cerium is added to it.[4] The materials used are typically ceramics for the substrate, oxides such as alumina or silica for the washcoat and noble metals for the catalyst. A schematic of such a catalytic converter is shown in figure 1.

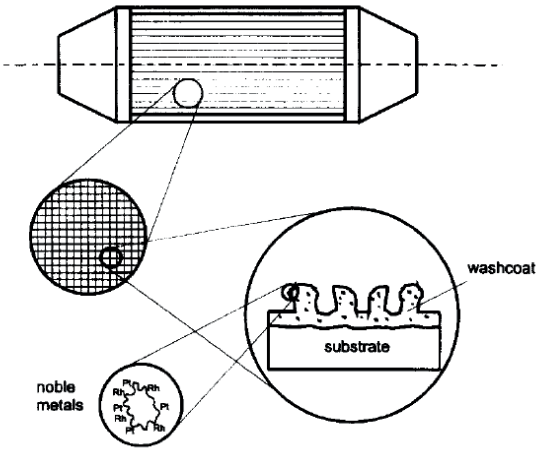

Figure 1: **3-way catalytic converter**
A schematic of the components of the 3-way converter used in cars, from Koltsakis et al.[4]

The reason for having only small particles of catalysts in the converter is cost. The most commonly used materials are platinum, palladium and rhodium, all expensive noble metals. Other materials have been tried for use as catalysts in the relevant reaction and some, like copper and cobalt oxides, show high activity for CO oxidation but low activity for hydrocarbon oxidation.[3] Their activity is furthermore strongly inhibited by sulphur compounds in the gas mixtures at temperatures below 500°C. One is left with the noble metals as the best catalysts to use in many applications.

The metals used in catalytic converters have different strengths and weaknesses when it comes to removal of pollutants. Pt is a common choice and is used to oxidise CO and hydrocarbons to CO_2 and water.[3] Pt is especially good at oxidising heavier hydrocarbons under conditions with excess oxygen available and is therefore often used in the catalysts for diesel engines.[5] Another advantage of Pt is its high thermal stability, which prevents the nano sized particles from sintering into larger particles.
Since the noble metals are sensitive to contaminants, expensive, and difficult to replace with cheaper alternatives researchers and engineers are constantly looking for ways in which the activity of catalysts can be improved or be made less sensitive to environmental conditions.

A persisting problem in the 3-way converter is the light-off temperature, that prevents effective operation when the engine is cold. Therefore it is very interesting that alloying platinum with iron has been reported to increase the catalytic activity of platinum for several reactions.[6;7;8;9] Different explanations have been offered for the increased activity, but one that has received much attention is the formation of an iron oxide layer on top of the platinum.
Catalysts are often employed in the way described above: nano sized particles embedded in a porous material (usually an oxide) and subject to fluctuating concentrations of various gases and, perhaps, particulate matter. This makes them difficult to study scientifically under realistic conditions. The facets the catalyst exposed to the gas, the number of defects and degree of surface roughness, the type and structure of the support material can all affect the reactivity of the sample. Since the substrate is usually a (non-conducting) oxide it cannot be studied with electron-based technologies like Low Energy Electron Diffraction (LEED) or X-ray Photo Emission Spectroscopy (XPS).

For these reasons simplified model systems are often used to study catalysis. To simplify the system large (∼cm) single crystals of the catalytic material are used. For platinum the most stable facet is the (111) crystal plane, which has a hexagonally close packed layer of Pt atoms at the surface. Because of its stability it can be expected to be the majority facet in real catalytic systems. To study the interaction of the catalytic metal and the substrate oxide the oxide is often grown on top of the metal single crystal. While this practice was introduced to study metal-substrate interactions it has been found that oxides on top of catalytic metals can in some cases increase the activity of the sample. An example is the ultra-thin iron oxide film grown on Pt(111). It consists of a single atomic layer of iron sandwiched between the Pt(111) surface and an oxygen surface layer, resulting in a (O - Fe - Pt ...) structure. Since this oxide film contains one atomic layer of iron and one atomic layer of oxygen it is referred to as a bilayer film.

First Sun *et al.*[10] and later Fu *et al.*[11] reported that the temperature for CO oxidation can be lowered for a Pt(111) surface if an ultra thin layer of iron oxide is grown on top of it.
In Sun's experiment the Pt(111) surface was initially completely covered with a bilayer film of iron oxide consisting of one atomic layer of iron and one atomic layer of oxygen ordered in a (O - Fe - Pt ...) fashion. The FeO/Pt(111) sample was then exposed to CO:O_2 gas mixtures of composition between 1:5 to 5:1 at a total partial pressure between 6-60 mbar (balanced by He to 1 bar) and temperatures between 400-450 K. The authors found that at 450 K the film dewetts in CO-rich conditions, meaning that part of the film looses contact with the substrate and forms "droplets" of iron oxide on the platinum. In contrast, the film is oxygen enriched and does not dewett at oxygen rich conditions. Under CO-rich conditions the dewetting was found to deactivate the catalyst while under O_2-rich conditions the most active phase was found to be the non-dewetted oxygen enriched surface. The increased activity at O_2-rich conditions was proposed to be due to part of the FeO/Pt(111) bilayer film reconstructing into an FeO_2/Pt(111) trilayer film with the extra oxygen reacting directly with CO to form CO_2, shown to the right in figure 2 a). The structure of the trilayer film was proposed to be (O - Fe - O - Pt ...).
In contrast, Fu used islands of FeO supported by Pt(111) as displayed in figure 2 b). The Pt(111) areas were then saturated with CO and the surface was exposed to O_2 at 10×10^{-8} mbar at room temperature which removed the CO by converting it to CO_2, something which did not happen for bare Pt(111).[11] The authors found that the rate at which CO was removed depended on the specific periphery density of the FeO islands, with a higher number of smaller islands (more periphery per area)

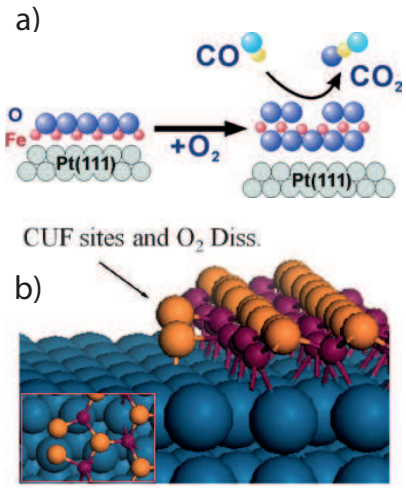

Figure 2: **CO oxidation on FeO_x**
a) proposed structure of the active FeO_2 film, from Sun et al.[12]*. b) Proposed active site from Fu at al., the iron atoms at the edge of the FeO patches.*[11]

removing CO faster than fewer larger islands (less periphery) at the same over all coverage. As the periphery of the FeO islands was shown to be iron terminated and consist of coordinatively unsaturated ferrous (CUF) sites (see figure 2 b)), the increased catalytic activity was attributed to these iron edges. This finding was rationalised by the lower adsorption energy of O_2 and CO on the CUF sites, it is lower for O_2 than for CO. This would give the O_2 molecules a site to adsorb on even when the Pt(111) surface is blocked by adsorbed CO. When the FeO islands were oxidised to FeO_2 the reactivity was lowered and activity was only observed at temperatures above 400 K. The group also manufactured nano sized Pt-Fe (4 weight percent Pt, 0.5 weight percent Fe) catalyst particles and tested their CO reactivity in 1% CO, 0.5% O_2 and 98.5% H_2 at 1 bar. The Pt-Fe catalyst showed stable performance and high CO conversion (>95%) for temperatures from RT to ~350 K, while the equivalent pure Pt nano particles only showed 70% CO conversion at ~470 K.[11]

Thus two different mechanisms for the low temperature CO oxidation for the FeO/Pt(111) system have been proposed: either an active FeO_2/Pt(111) trilayer reacting directly with CO (Sun *et al.*) or O_2 adsorption on coordinatively unsaturated ferrous sites at the Pt(111) FeO boundary. The studies were carried out at different temperatures and pressures and the behaviour of the FeO film in the two cases might have been rather different, which makes it difficult to confirm or rule out either of the proposed mechanisms. It is possible that both mechanisms are correct and that they become relevant at different temperatures, pressures and chemical environments. To get a better understanding of how the FeO/Pt(111) system behaves under different temperatures and pressures a more in-depth study is warranted.

The bi-layer FeO oxide film on Pt(111) was first described by Vurens *et al.* in 1988 and is prepared by evaporating iron onto a Pt(111) surface and oxidising it at elevated temperatures.[14] The iron in the oxide binds strongly to the platinum substrate and the deposited iron grows into iron oxide in a layer-by-layer fashion with oxygen in the outermost layer, illustrated in figure 3 a) and b). The growth method described above is a robust way to produce oxide layers of atomic thickness on metal substrates. Structurally, the FeO film consists of hexagonally close packed layers of iron and oxygen, similar to the (111) plane in bulk FeO (Wüstite). The Pt(111) substrate surface also has a hexagonally close packed structure but the lattice constant of the FeO layer (3.1 Å) is ~12% larger than that of Pt(111) (2.77 Å) and the FeO lattice is also rotated by 0.6°relative to the Pt(111) lattice. These two facts give rise to a characteristic pattern in LEED images with the main diffraction spots from the FeO(111) hexagonal structure surrounded by a rosette of six secondary spots (shown in figure 3 d)). The rosette is caused by the six-fold rotational symmetry of the FeO/Pt(111) super cell. A moiré pattern is also visible in the ball model of the FeO/Pt(111) system in figure 3 e) where it can be seen that the lower left part of the FeO/Pt(111) super lattice is lighter while the upper right half is darker, depending of the location of underlying Pt atoms relative to the FeO lattice. Thermally the FeO film is stable up to temperatures of 1100 K, above that temperature segregation of Fe to the Pt bulk sets in.[14]

Chemically, the FeO film is inert towards CO and H_2O adsorption in UHV conditions. Thus, it can be said that the FeO overlayer is in general very stable and resistant to decomposition, though the dewetting reported by Sun *et al.* discussed above should be kept in mind.

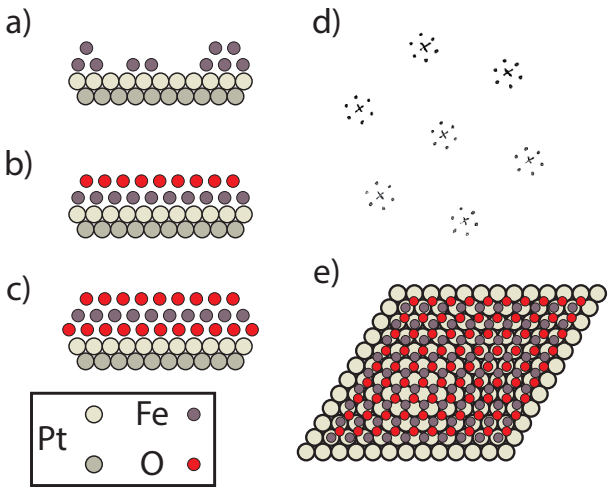

Figure 3: **Structure of the FeO/Pt(111) system** *a) iron deposited on Pt(111). The FeO bilayer (b) and trilayer (c) film on Pt(111). d) schematic of the LEED pattern from the FeO bilayer film from Vurens et al.*[13] *e) the FeO(111) unit cell on a Pt(111) substrate.*

If exposed to O_2 at sufficient temperatures and pressures (∼mbar) the FeO film can form a new FeO_2 trilayer film, which has been characterised in detail with XPS by Johansson *et al.*.[15] The binding energies used to characterise the FeO and FeO_2 overlayers were O 1s, Fe 3p and Pt 4f. When the FeO film changes to FeO_2 the O 1s peak changes from a single peak at 529.4 eV to three peaks at 528.5 eV, 529.0 eV and 531.0 eV that correspond to surface oxygen, interface oxygen and surfacce hydroxyl groups respectively in the FeO_2 film. The LEED image of the FeO_2 film retained the florette patterns caused by the moiré structure and so the overall structure was found to be similar to that of FeO/Pt(111). The authors found that the FeO_2 film hydroxylises very readily, even when the FeO film was oxidised with pure O_2, NO_2 or atomic oxygen.[15]. It was concluded that even the small H_2O impurities present in the gases or in the chamber were enough to hydroxylate the FeO_2 film and it was therefore concluded to be highly active for water dissociation. It was also observed that the hydroxyl groups become visible at the onset of growth of the FeO_2 layer and it is proposed that water is closely connected to, perhaps necessary for, the growth of the FeO_2 film. For this reason, the authors expect the FeO/FeO_2 boundary to be the active site for water dissociation.
So far no FeO_2 film on Pt(111) with complete coverage has been observed experimentally, only islands of FeO_2/Pt(111) accompanied by bilayer FeO/Pt(111) have.[16] This was explained by considering the energy cost of inserting a layer of oxygen in between the Pt and the Fe in different points in the moiré super cell (see figure 3 e)). It has been found that the oxygen enriched FeO_2 film forms most easily when the Fe atoms are located above ffc hollow sites of the Pt substrate atoms.[17] This would correspond to the lower left part of the FeO/Pt(111) super cell in figure 3 e).

As mentioned previously, several explanations exist for the observed low temperature CO oxidation activity of the FeO_x/Pt(111) system, with the formation of an active FeO_2 trilayer and the exposure of active iron atoms on the FeO-Pt(111) boundaries are both attractive explanations.

This thesis aims to shed light on the changes the FeO/Pt(111) system goes through during CO oxidation. The film was made to switch between FeO/Pt(111) bilayer and FeO_2/Pt(111) trilayer by periodically varying the CO:O_2 ratio of the gas exposed to the sample. Studying this phase change will be worthwhile in itself and can also be used to test the hypothesis of Sun *et al.* with the active FeO_2 trilayer for CO oxidation. Also, the behaviour of the catalytic system during the phase change may well be different from the steady sates that have been studied so far. Introducing a varying gas composition and phase changes will also make the model system more similar to a real catalyst, which is exposed to gas mixtures that may vary in time and on which phase changes may occur.
The main technique for my work has been Ambient Pressure X-ray Photo Emission Spectroscopy (APXPS), which allows pressures of ∼1 mbar in the reaction chamber. This makes it possible to record spectra from the sample surface and the gas just above it simultaneously. With this information it is possible to correlate presence of gases (like CO_2 for example) and the surface state of the sample. Through the gas phase signals in the spectra work function shifts of the sample can also be tracked (more information about this in the next section).
The activity of the FeO_x/Pt(111) system for CO oxidation was measured on two occasions during the course of this work. The first time a clear difference in activity was observed for Fe_xO/Pt(111) relative to a clean Pt(111) reference. The second time (roughly 4 months later) there was no clear difference in activity of the FeO_x/Pt(111) and Pt(111) samples. The light off temperature of the platinum was also different in the two measurement sessions. As we judge it more likely that the first measurement session produced inaccurate results only data from the second session are treated in most of the thesis, results from the first session are included in the end of the results and discussion section.

2 Experimental techniques

All types of photo emission spectroscopy utilise the photoelectric effect to induce the emittance of electrons from a sample, which can be analysed to extract information about the sample. In X-ray Photo Emission Spectroscopy (XPS) deep core level electrons are emitted from the atoms in the sample and their kinetic energy is measured. For solid materials the binding energy is defined as the difference in energy between the bound energy and the Fermi energy, the highest occupied level. As the photon energy is known one can calculate the binding energy as:

$$E_{kin}^{Solid} + E_B = E_{h\nu} - \Phi_A \tag{1}$$

where $h\nu$ is the energy of the incoming photon, E_B is the binding energy and Φ_A is the work function of the electron analyser.

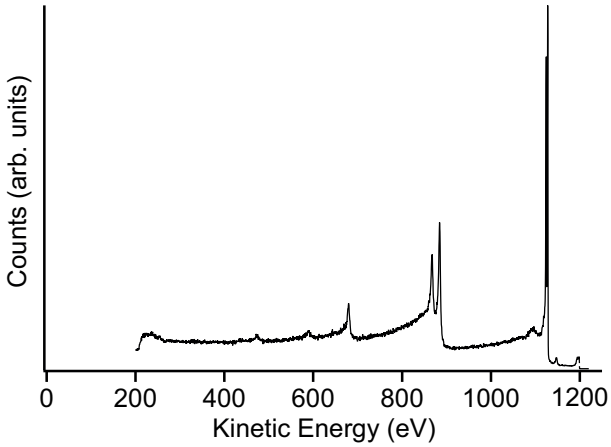

Figure 4: **Survey spectrum**
XPS spectrum from a clean Pt(111) crystal.

In XPS the photon energy $E_{h\nu}$ is kept constant while the number of emitted electrons is measured as a function of their kinetic energy. By using equation 1 it is possible to convert the measured kinetic energy into binding energy for the electrons. An example spectrum of a Pt(111) crystal taken with photon energy 1200 eV is shown in figure 4.
To deal with the work function in equation 1 the kinetic energy for the Fermi level is also measured. The binding energy of the Fermi level is by definition equal to zero, so the kinetic energy becomes:

$$E_{kin}^{FE} = E_{h\nu} - \Phi_A \tag{2}$$

By combining equations 1 and 2 it is possible to calculate the binding energy as:

$$E_{kin}^{FE} - E_{kin}^{Solid} = E_{h\nu} - \Phi_A - E_{h\nu} + E_B + \Phi_A = E_B \tag{3}$$

which is independent of the analyser work function Φ_A, as illustrated in figure 5.
The peaks in figure 4 originate from photoelectrons excited from elemental specific core levels of the atoms in the material under investigation. For example, in figure 4 only peaks originating from Pt binding energies are seen. This characteristic of XPS makes the technique well suited to determine the chemical composition of a sample and for this reason XPS is often referred to as Electron Spectroscopy for Chemical Analysis (ESCA). Furthermore, the binding energies of the elements are affected by the local electron structure around the atom, often referred to as the chemical shift. For example, if an ionised metal atom is bound to oxygen it will have a slightly shifted core level as compared to metallic metal atoms. This makes XPS elemental and chemical sensitive, one of the great strengths of XPS.

The spectra originating from atoms and molecules on the surface and the spectra originating from gas phase molecules are treated differently, as illustrated by figure 5 and 6.

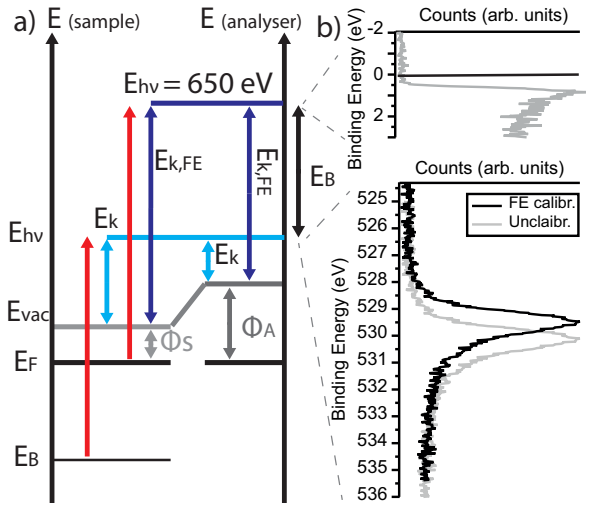

Figure 5: **Photo emission from a solid**
a) Photo emission from a solid sample.
b) XPS spectra from a Pt(111) surface in 0.6 mbar O_2*, Fermi edge (top) and O 1s region (bottom).*

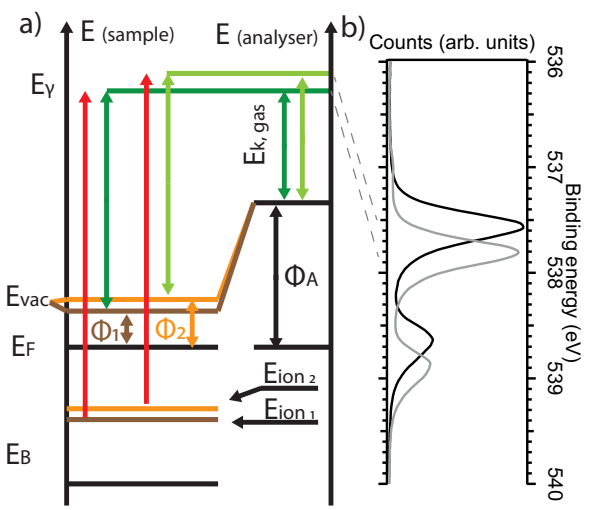

Figure 6: **Photo emission from a gas**
a) Photo emission from gas phase molecules for two different work functions, Φ_1 *&* Φ_2*.*
b) XPS spectra for a Pt(111) crystal in 0.6 mbar O_2*.* $E_{h\nu}$ = 650 eV.

After the photoelectrons are emitted from the solid sample their kinetic energy is affected by the sample work function Φ_S. It can be seen in figure 5 that Φ_S does not affect the kinetic energy of the photoelectrons after they reach the analyser, only Φ_A does. As previously shown Φ_A does not affect the difference $E_{kin}^{FE} - E_{kin}^{Solid}$ used in eq. 3 to calculate the binding energy.

Looking at the spectrum for gas phase O_2 in figure 6 b) the biggest difference compared to the chemisorbed O in 5 b) is a shift of ∼8 eV towards higher binding energies. This is a chemical shift caused by the oxygen no longer being bound to the Pt metal but rather to another oxygen atom as O_2. Two shifts within the O_2 gas phase can also be seen. The smaller shift (∼ 0.3 eV) is caused by that the reference point for the electrons from the gas phase is the vacuum level rather than the Fermi energy. The vacuum level can be expressed relative to the Fermi energy like $E_{vac} = \Phi_v$ where Φ_v is a space dependent potential. The additional potential for electrons from gas molecules can then be written as: $Pot^{gas} = \Phi_A - \Phi_v$. The equation for the kinetic energies is then:

$$E_{kin}^{Gas} = E_{h\nu} - E_{ion} - (\Phi_A - \Phi_v) \tag{4}$$

The vacuum level is determined by the potential surrounding the molecule and if, for example, the gas becomes charged or some potential is introduced the measured kinetic energy from the gas molecules will change. If the molecule is very near to the surface of the sample it will be approximately equal to the work function of the sample: $\Phi_v \approx \Phi_S$ and the kinetic energy from molecules is then:

$$E_{kin}^{Gas,surface} \approx E_{h\nu} - E_{ion} - (\Phi_A - \Phi_S) \tag{5}$$

Thus, it can be seen that if the gas phase molecule is near the surface its apparent binding energy will change if the work function of the surface changes. An example of this is seen in figure 6 for work functions Φ_1 and Φ_2. In this way changes in sample work function can be probed by measuring on gas just above the surface.

The final state of the ionised molecule can also affect the observed binding energy obtained with photo emission spectroscopy. This is the cause for the larger shift within the O_2 spectrum, seen in figure 6 b). In neutral O_2 the spins of the (two) 1s electrons will be orthogonal and not contribute any magnetic moment to the molecule but when one of the 1s electrons are removed the resulting hole will have a spin of $s = 1/2$. If the valence electrons of the molecule have a net magnetic moment (as is the case for O_2, it has $S = 1$) the spin of the core 1s hole can couple to the valence magnetic moment. For O_2^+ this can result in the total magnetic moments $|1 - 1/2| \leq J \leq |1 + 1/2| = 1/2, 3/2$ with different energies. This gives rise to two observed binding energies for the single 1s level, separated by 1.1 eV. This split of the O 1s level will be observed in the experiments in this thesis.

To evaluate the intensity that can be expected from a certain atomic level the photon absorption probability and the electron range also has to be considered. For 1s levels the probability for photon absorption is maximised when the photon energy coincides with the binding energy of an electron and decreases as the photon energy becomes larger than the binding energy. An example for the 1s core level in oxygen, which has a binding energy of ~540 eV, is shown in figure 7.

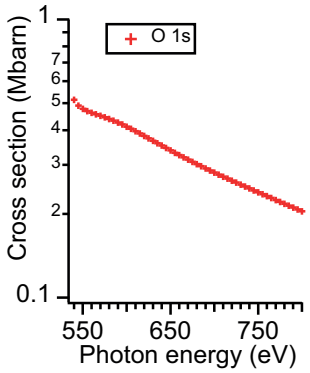

Figure 7: **Cross section** *Photoelectric cross section for O 1s, from Elettra.* [18]

When electrons are emitted from the sample, they have to reach the detector without scattering inelastically to be useful as probes, which brings us into the discussion of electron mean free path. For the electron kinetic energies used in XPS (~100 eV) the main reason for electron scattering is electron-electron collisions. At these energies the collision probability depends mostly on the electron density in the material it travels through. This is what makes XPS so surface sensitive: for solids the mean free path of electrons at these energies are about 2-10 Å. Electrons from bulk atoms have a high probability to scatter as they travel through overlying atomic layers and as a result only significant amounts of electrons from the topmost atomic layers reach the detector undisturbed.

The same characteristic that makes XPS surface sensitive also limits the pressures that can be used in the analysis chamber. The electron mean free path in gases is ~1 mm at 100 eV kinetic energy in 1 mbar N_2 gas, which is much shorter than the size of the electron analyser (whose detector also needs to be at UHV). To overcome this problem one places a small aperture close to

the sample surface and pump the compartment behind the aperture (the pre-lens) heavily so that it is kept at $\sim 1 \times 10^{-3}$ mbar. In this way the photoelectrons only have to pass a short distance through the mbar gas above the sample (typically $\sim$ 1 mm) before they enter the lower pressure regions of the pre-lens and the electron analyser. This Ambient Pressure X-ray Photo Emission Spectroscopy (APXPS) technique was developed to able to measure on samples at mbar pressures.

In order to keep the pressure in the electron analyser low enough it is divided into several compartments that are each connected and pumped separately, differential pumping. For my experiments I used a HIPP-3 ambient pressure analyser from ScientaOmicron, figure 8 a) shows a schematic of the HIPP-3 electron analyser. The compartments of the analyser are referred to as pumping stages in figure 8 a) and each pumping stage is separated from adjacent stages with small apertures. The small apertures allow the pressure to be increasingly lower in each pumping stage and this is necessary as the electron detector in the last pumping stage is pressure sensitive.

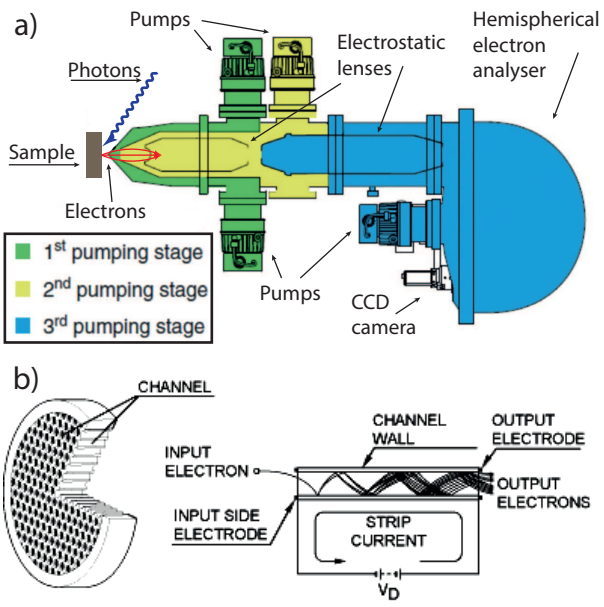

Figure 8: **Electron analyser**
a) HIPP-3 electron analyser, adapted from[19]
b) Schematic of an MCP, from DM Photonics.[20]

The way in which the electron analyser discriminates between electrons with different kinetic energy is by bending their path with an electrostatic field. In the HIPP-3 this field is set up with a hemispherical metal shell. The force on the electrons is equal and constant and the curvature of their paths will depend on their speed. This means that electrons with less kinetic energy will be bent more and electrons with higher kinetic energy bent less. Thus, only electrons within a certain range of kinetic energy will have the right curvature to hit the detector.
Thanks to pre-retarding the electrons before they enter the hemisphere, the HIPP-3 analyser can achieve great energy resolution. The pass energy is the energy the electrons have when they enter the hemisphere and determines the maximum energy resolution.
The HIPP-3 analyser uses a Multi Channel Plate (MCP) electron detector, figure 8 b) shows an example of one. It consists of two conducting plates separated by an insulator and filled with holes. A high voltage ($\sim$1 kV) is applied over the plates. When an electron from the sample hits the wall of one of the holes it releases additional electrons from the material between the

plates. They are then accelerated by the high voltage, collide with the walls, release more electrons which results in an electron avalanche process. After the multiplied electrons have passed through the MCP plates they reach a phosphorescent screen. When they strike the screen, the material produces light which is captured by an external CCD camera through a view port.

The energy range the whole MCP plate can capture in one shot is ∼10% of the pass energy. With typical pass energies this results in an energy resolution better than 10 meV. Two types of spectra can be recorded with the electron analyser: swept spectra and snapshot spectra. In swept spectra the retarding voltage is swept over a range of energies and spectra are recorded continuously by the MCP. Electrons with a certain original kinetic energy will then also be swept over the MCP and the final spectrum is created by integrating the signals for each kinetic energy over all channels. This makes it possible to eliminate any differences in channel sensitivity as all measured kinetic energies will have hit all the channels of the MCP at some point during the sweep.
In snapshot mode the MCP records spectra with a certain repetition rate (maximum rate is approximately ∼10 Hz in my case) and no energy sweep is performed. This limits the energy range that can be visualised in each snapshot. The energy range of the MCP is ∼10% of the pass energy so for typical pass energies of ∼100 eV this means an energy window of ∼10 eV. This makes it impossible to record for example O 1s (∼535 eV) and C 1s (∼290 eV) spectra simultaneously. Another effect of the lack of a sweep is that the signals cannot be integrated to account for local differences in detector sensitivity. This generally causes signals in the middle of the window (and in the middle of the circular MCP plate) to be more intense than energies in the edge of the window. If some of the MCP pixels are damaged this would also cause an irregular change in signal strength. These effects will generally have to be accounted for during the post-recording data treatment of the spectra.

The post-recording data treatment was done in IGOR 7 Pro[21] and most scripts for data treatment I made myself from scratch using IGOR's basic built-in functions. Scripts were made to calibrate spectra, remove background, scaling, automated fitting of time resolved image plots, alignment of periodic signals, binning and more.

3 Results and discussion

FeO/Pt(111) and FeO_2/Pt(111) characterisation

In order to confirm that we had grown the FeO/Pt(111) and FeO_2/Pt(111) films correctly a characterisation of the surface was carried out before the CO oxidation experiments. The characterisation was done using XPS and LEED and the values obtained compared with literature.

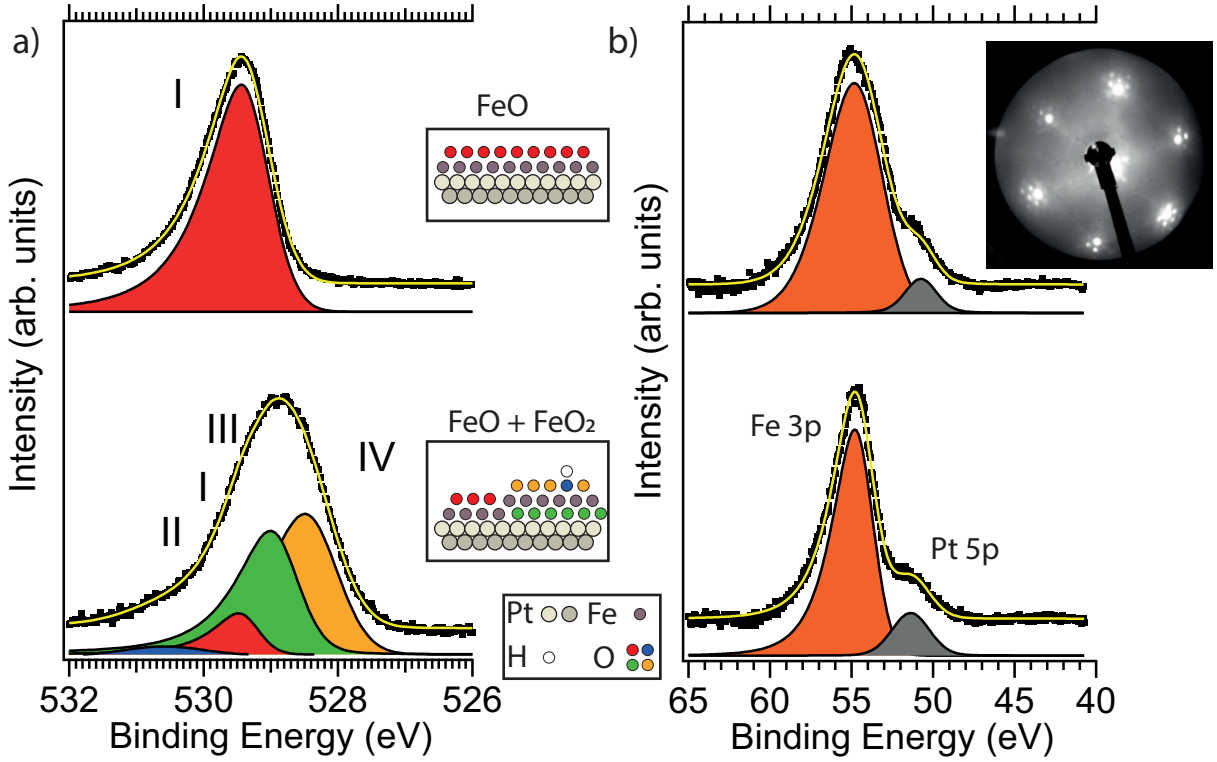

Figure 9: **Fingerprints of FeO and FeO_2**
a) O 1s Spectra of the FeO_x/Pt(111) film at room temperature and UHV (top), 140°*C and* 0.6 mbar O_2 *(bottom). b) Spectra of Fe 3p and Pt 5p at room temperature and UHV (top) and at* 140°*C and* 0.6 mbar O_2 *(bottom). In b) a LEED image of the FeO/Pt(111) sample is inset.*

Figure 9 shows the O 1s and Fe 3p spectra of the FeO/Pt(111) film measured at UHV conditions and room temperature in the top panels and the FeO_2/Pt(111) film in 0.6 mbar of O_2 at 140°C in the bottom panels, respectively. For these fingerprint spectra a Shirley background was subtracted from the O 1s peaks. For the Fe 3p peaks a third degree polynomial function was used as background, as a nearby peak at higher binding energy made using a Shirley background difficult. All peaks were fitted with asymmetric Voigt peaks. The O 1s I component is attributed to oxygen in the FeO bilayer. In the FeO_2 trilayer the weak II component is attributed to hydroxyl groups, III to inter-facial oxygen and IV to surface oxygen. The experimentally determined

binding energies are listed in table 1. References for the FeO/Pt(111) and FeO_2/Pt(111) taken from literature[15] are included in table 1.

Experimentally determined binding energies:							
O 1s:	I	II	III	IV	Fe 3p		Pt 5p
FeO:	529.4 eV	-	-	-	54.8 eV		50.8 eV
FeO_2:	529.5 eV	530.6 eV	529.0 eV	528.5 eV	54.8 eV		51.4 eV
Reference values from Johansson *et al.*[15]							
O 1s:	I	II	III	IV	Fe 3p (max)	Fe 3p (mid)	Pt 5p
FeO:	529.4 eV	-	-	-	54.1 eV	55.0 eV	51.4 eV
FeO_2:	-	531.0 eV	529.0 eV	528.5 eV	54.6 eV	55.2 eV	51.4 eV

Table 1: Peaks in FeO/Pt(111) and FeO_2/Pt(111)

Starting with the FeO/Pt(111) film evidence for the formation of the FeO(111) phase comes from the binding energy of the O 1s (I) component in the room temperature spectrum in figure 9 a) and the rosette pattern in the LEED image in b), which both match literature values very well.[22;23]
For the FeO_2/Pt(111) film the binding energies of the O1s I, III and IV components also match very well with the literature values, showing that also the FeO_2 trilayer was formed like intended. In our spectra component II (hydroxyl groups) is less intense and component IV (interface oxygen) is more intense. From this observation we conclude that our FeO_2 film is less hydroxylated than the one in the reference study, which is interesting as the FeO_2 film is hydroxylated very easily in the reference study. A possible reason for the difference lies in the mechanism for heating the sample; in Johansson *et al.* the sample was heated indirectly through the sample holder while in our study the sample was heated directly with a laser. Heating the sample holder and surrounding material could cause degassing of for example H_2O from the chamber and it has also been reported that such indirect heating can cause reactions involving the chamber material[24]. The shifts of the O 1s peak(s) between FeO and FeO_2 is supported by theoretical calculations by Giordano *et al.*.[25]
The Fe 3p and Pt 5p peaks contain less information than the O 1s peaks. The shift in the Fe 3p peak is small, but the intensity ratio of Fe 3p and Pt 5p can be used to determine the iron content of the sample surface. If the intensity of the Fe 3p peak decreases relative to the Pt 5p peak it would mean that iron is lost from the surface, for example by segregating into the bulk. As the Fe 3p to Pt 5p ratio stays constant during the FeO/Pt(111) to FeO_2/Pt(111) transformation we have to conclude that the iron stays in the surface layer.

From these observations we conclude that our FeO and FeO_2 spectra agree qualitatively with literature values. Further, we note that the O 1s spectra of the FeO and FeO_2 look quite different, and it is therefore relatively easy to distinguish between the two phases at reaction conditions. Even if the time resolved spectra are much noisier than the high resolution spectra in figure 9

and the individual components are not possible to fit accurately, the overall shift between lower or higher binding energies in the O 1s spectra can still be distinguishable. Finally, the Fe 3p + Pt 5p can be used to check the iron content of the sample surface at reaction conditions.

Pulsed APXPS experiments

During the CO oxidation experiments two types of APXPS spectra were recorded: surface spectra and gas phase spectra. The surface spectra probe core electrons from the surface of the sample and molecules in the gas just above the sample surface (see fig 10 a). For recording the gas phase spectra the sample was retracted by 0.3 mm relative to the position used in the surface spectra. This is illustrated in figure 10 b) where the position used for surface spectra is marked in red. Retracting the sample causes the synchrotron light to hit the surface beside the analyser cone and the electrons from the surface, therefore, miss the aperture of the analyser. Thus, only electrons from the gas above the sample are able to enter the electron analyser in this retracted position. Electrons from bulk atoms that scatter inelastically is the main source for the background in XP-spectra. Without a surface signal the background disappears and the intensity of the light can be increased substantially without saturating the detector. In our case it was possible to increase the signal strength by a factor 15, improving the signal to noise ratio significantly.

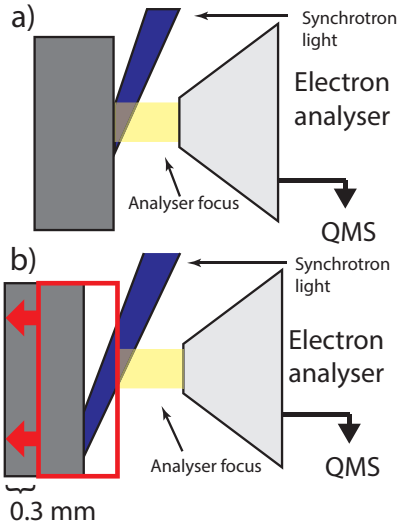

Figure 10: **Electron analyser**
a) sample in surface spectra recording position. b) sample in gas phase spectra recording position.

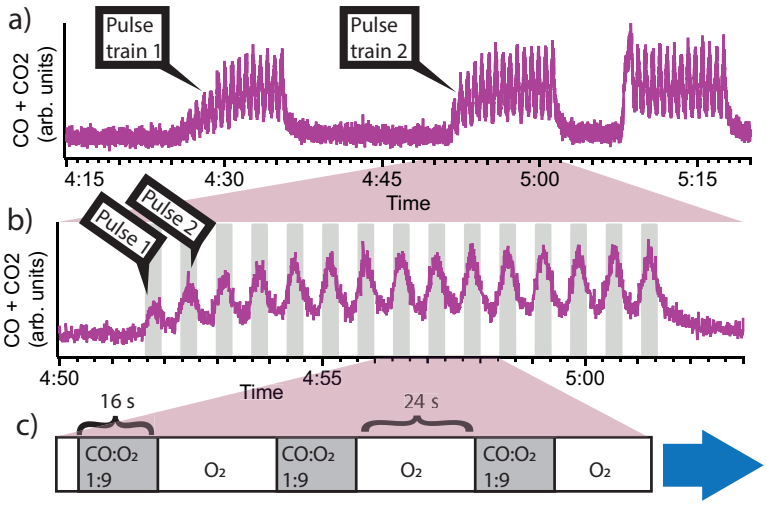

Figure 11: **Pulse trains and pulses**
a) the combined signal from CO and CO_2 from the FeO/Pt(111) measurements at 160°*C with QMS. b) a close-up of one of the pulse trains from a). c) an illustration of the composition of the pulses sent to the sample.*

During the pulsed experiments CO was oxidised with O_2 to CO_2. All experiments were carried out at 160°C. The samples were kept in 0.6 mbar of O_2 created by an inlet gas flow of 10 sccm O_2 into the AP Cell. The CO oxidation was then performed by sending in 16 s pulses of 1:9 CO:O_2 mixture separated by 24 s of pure O_2. Fifteen such pulses were used in a pulse train. An overview of the gas pulses used in the experiments is shown in figure 11. Panel (a) shows the summed CO and CO_2 signal from the analyser measured with the Quadrupole Mass Spectrometer (QMS) and shows three pulse trains used in the FeO/Pt(111) measurements. In panel (b) the second pulse train is magnified so that the individual pulses can be seen. An illustration of the composition of the pulses is shown in panel (c).
As can be seen in figure 11 b), the shapes of the pulses are not sharp by the time they reach the sample. The original shape of the pulses is not known, and they may have been sharper than or as diffuse as the ones observed in 11 (b). However, the intensity of the sum of CO and CO_2 partial pressures during a pulse is larger than the intensity between pulses by a factor of almost four. Therefore, the pulses can still be considered to be adequately well defined in time for our experiments.

APXPS gas phase spectra of FeO/Pt(111):

The gas phase spectra below were recorded with a repetition rate of 8.5 Hz and have been binned four times, making the effective repetition rate ~2 Hz. All image plots are recorded with the sample retracted 0.3 mm from the normal measurement position. Therefore, the images show the spectra originating from the gas phase 0.3 mm above the sample.

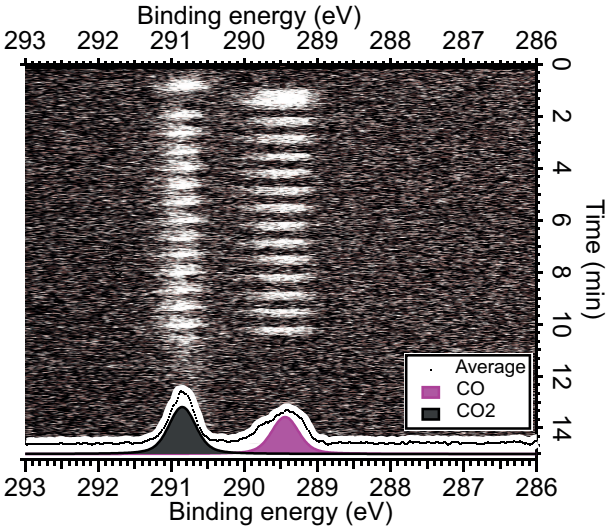

Figure 12:
C 1s gas phase spectra on FeO_2/Pt(111)
The spectra show pulses of CO being sent to the sample in 0.6 mbar O_2 *at* 160°C. *The time averaged spectrum of the image plot is inset.*

Figure 12 shows an image plot of C 1s acquired during one pulse train for Pt(111) covered with one ML FeO_x at 160°C. In the bottom of the panel the averaged spectrum is inset. The peak at ~ 291 eV is attributed to gas phase CO_2 and the peak seen at ~ 289.5 eV is attributed to gas phase CO.

In the C 1s image plot in figure 12 we observe pure CO_2 in the first pulse of the pulse train, indicating complete combustion of CO to CO_2, followed by a pulse of pure CO. After the first two pulses the behaviour of the sample becomes more regular. While CO_2 is produced throughout the rest of the pulse train conversion is partial, as can be seen by the presence of both CO_2 and CO in figure 12. After the pulse trains have finished (and no more CO is present) a weak CO_2 "tail" signal can be seen in figure 12 (after ~ 11 min).
The pure CO in the second pulse in the C 1s image plot was never observed for any other pulse train and is therefore not discussed further. It is noted that during the experimental session the time it took for CO conversion to become partial varied slightly from pulse train to pulse train. If the sample had recently been exposed to CO the CO_2 production became partial much earlier than if the sample had been in a pure O_2 flow for a longer period of time. Pulse trains that were sent after longer periods of pure O_2 flows also had lower CO + CO_2 concentration during the first few pulses as measured by the QMS on the gas from the electron analyser. All these observations suggest a memory effect associated with the dosing of CO that affects the intensities of the gas pulses and as an effect how many pulses it takes before CO_2 conversion becomes partial. To summarise, in figure 12 CO conversion is complete for the first pulse of the pulse train and becomes partial after the second pulse. When CO conversion has become partial it stays partial for the remainder of the pulse train.

Figure 13 a) shows an image plot of O 1s acquired during one pulse train for Pt(111) covered with one ML FeO_x at 160°C. The average spectrum is inset in the bottom. Panel b) shows the fitted apparent binding energy of the strongest O_2 component, divided into the active (red) and inactive (green) states of the sample. The apparent binding energy in b) has been used in panel (c) which shows the average spectra of the image plot in (a) for the active (red) and inactive (green) states of the sample. The O 1s image in a) and average spectra in a) and c) are in log scale to make weak peaks visible.

In the O 1s image plot in figure 13 a) the two strong shifting peaks at ∼ 538 eV and ∼ 539 eV are both attributed to the O_2 doublet. The peak at ∼ 536 eV is attributed to gas phase CO_2 and the weak peak at ∼ 537 eV is attributed to CO. As seen in panel b) the apparent binding energy of the O_2 doublet peaks oscillate back and forth during the pulse train, which makes an ordinary average spectrum of all spectra in the image plot inaccurate. Therefore, in c) two average spectra for the O 1s image plot has been made showing lower (red) and higher (green) O_2 doublet apparent binding energy. This method is used later for all O 1s spectra.

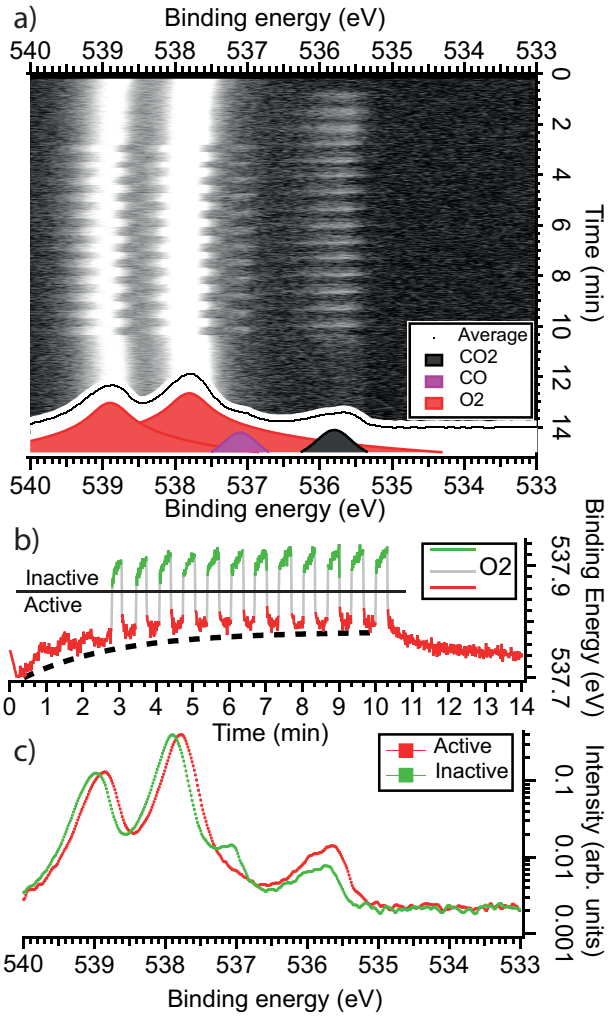

Figure 13:
O 1s gas phase spectra on FeO_2/Pt(111)
The spectra show pulses of CO being sent to the sample in 0.6 mbar O_2 *at* 160°C. *a) snapshot APXPS spectra with the time averaged spectra inset an the bottom. b) the fitted binding energy of the strongest O_2 peak. c) the time average spectra of the active (red) and inactive (green) phases respectively.*

The production of CO_2 seen in the O 1s image in figure 13 a) qualitatively matches the production seen in figure 12: CO_2 is produced throughout the entire pulse train with complete conversion in the beginning of the pulse train and partial for the remainder. There is a difference in how many pulses are completely converted to CO_2 before CO becomes visible which is attributed to the memory effect discussed previously.

The shifts of the gas phase peaks can be analysed to determine changes in the work function of the sample, as discussed in the introduction.
On a long time scale (minutes) the gas phase peaks in figure 13 a) shift to higher values during the course of the pulse train (indicated by a dashed black line in figure 13 b)). The shift is fastest in the beginning of the pulse train and stabilises after a few pulses. After the pulse train has ended the O_2 doublet shifts down slowly to lower binding energies again. Therefore, the surface must change phase slowly during oxidation of CO and is then changed again when the pulse train has passed. At least during the first few pulses this change does not appear to affect CO_2 production, which is complete.
On a short time scale (seconds) there is a fast oscillatory shift of the gas phase peaks seen during the pulse train. The shift is indicated with colour coding and the states are separated with a solid black line in figure 13 b). This shift means that the work function of the sample changes rapidly between two values, indicating two different surface states of the sample. The periodic shift of the O_2 doublet is ~ 0.11 eV to higher binding energies with the first shift occurring after the first few pulses, at ~ 3 min in figure 13 b). The period of the shift is ~ 40 s, the same period as the gas pulses (16 s 1:9 + 24 s 0:10 CO:O_2 mixture). Therefore, the oscillation is interpreted to be caused by the gas pulses. In the average spectra in figure 13 c) it can be seen that CO is present only in the state corresponding to higher apparent binding energy while CO_2 is present in the spectra for both surface states. The conclusion is that the surface corresponding to higher O_2 binding energies adversely affects CO_2 production. The state with higher apparent binding energy is therefore labelled "inactive" while the state with lower apparent binding energy is labelled "active".

To summarise, CO_2 production is observed on the FeO_2/Pt(111) sample with complete CO conversion for the first few pulses followed by partial conversion. The sample undergoes a slow work function change during the course of the pulse train as well as a fast oscillatory change during the pulse train. CO is only visible for the state corresponding to higher apparent binding energy while CO_2 is visible in both states.

In figures 12 and 13 it was concluded that CO conversion was partial for most of the pulse train. It is not seen in the previous figures whether the CO conversion is constantly partial or if it varies in time. In order to get a clearer picture of the CO and CO_2 concentrations it is desirable to improve the signal to noise ratio of the data and study the transition between the active and inactive states. Therefore the image plots from the last pulses of the pulse train have been added up in figure 14 and 15. In figure 14 the position of the CO signal has been used to align the pulses while in 15 the apparent O_2 binding energy has been used.

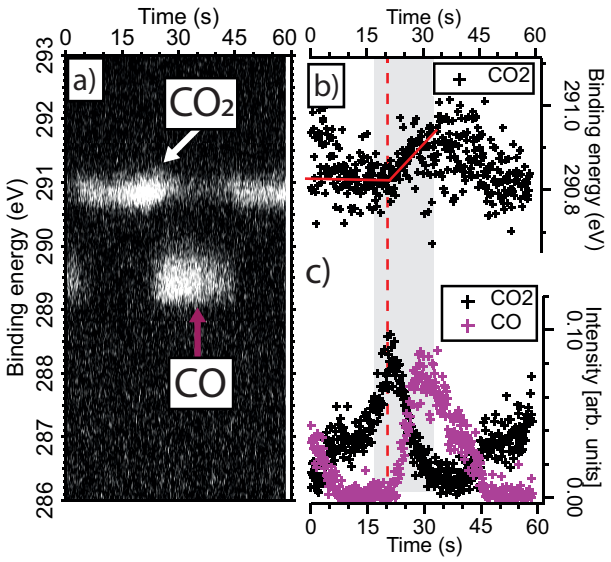

Figure 14: **C 1s gas phase spectra of one CO pulse on FeO/Pt(111)**
The image (a) shows a pulse of CO being sent to the FeO/Pt(111) sample at 0.6 mbar *at* 160°*C. b) the fitted CO_2 apparent binding energy. c) the CO and CO_2 intensities from the fitted peaks.*

The image from figure 12 has been used to add spectra from the last 12 pulses together and are shown in figure 14. Panel a) shows the resulting C 1s image plot of a single CO pulse. Contrary to in figure 12 the images are not binned in time and have a displayed repetition rate of 8.5 Hz. Panel b) shows the fitted binding energy of the CO_2 component and panel c) shows the integrated intensities of the fitted CO and CO_2 peaks. The grey box marks the length of the CO pulse.

The first observation to make from figure 14 is the mismatch between the CO and CO_2 intensities: CO is absent until the CO_2 signal starts to decrease, indicated by a red dashed line in figure 14 b) and c). This shows that CO conversion is complete in the beginning of the pulse only to cease completely after a while. The second observation is that the CO_2 apparent binding energy starts to shift to higher values at the same point, again indicated by the dashed red line.
In summary, during a CO pulse with partial conversion the conversion is originally complete, becomes partial and then ceases. This change in CO_2 production is accompanied by a work function shift.

In the same fashion that the pulses in the C 1s image plot has been summed up the pulses in the O 1s image plot can be summed as well. This is done in figure 15.

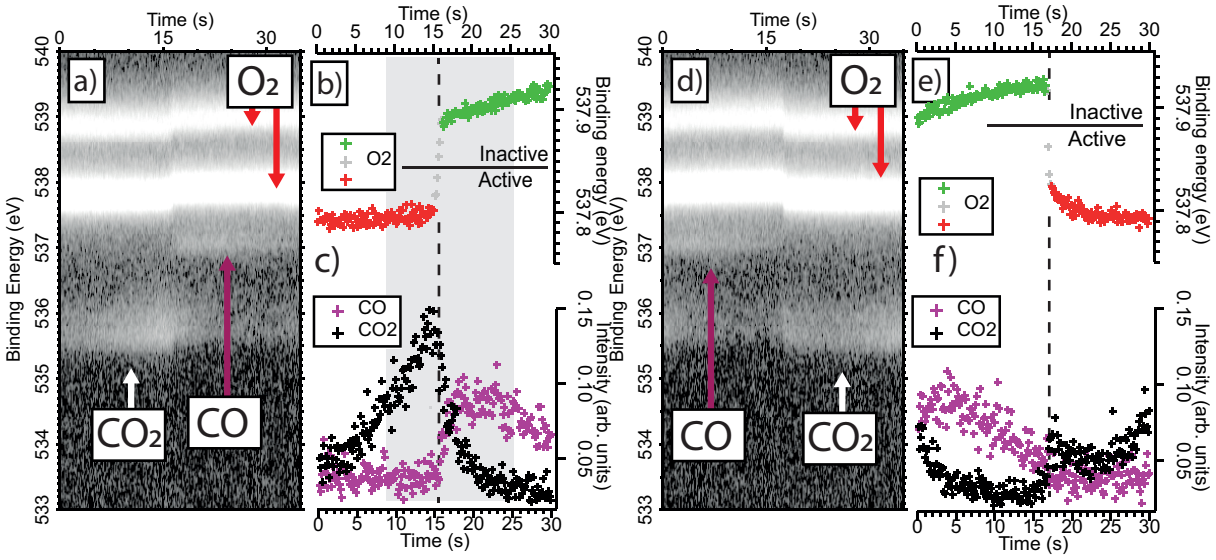

Figure 15: **O 1s gas phase spectra during the O_2 shift on FeO/Pt(111)**
The log scale images in a) and d) show the FeO/Pt(111) sample at 0.6 mbar *at* 160°*C switch from active to inactive (a) and from inactive to active (d) phase respectively. The grey box shows the pulse width. b) and e) show the fitted apparent binding energy of the strongest O_2 component. c) and f) show the CO and CO_2 intensities from the fitted peaks.*

The image from figure 13 a) has been used to add spectra from the last 12 pulses together and are shown in figure 15. Panel a) and d) show the resulting log scale image plots showing a) an increase and d) a decrease in peak position for the O_2 doublet. Contrary to in figure 13 the images are not binned in time and have a displayed repetition rate of 8.5 Hz. Panel b) and e) show the fitted binding energies of the strongest O_2 component with the active state marked in red and the inactive state in green. Panel c) and f) show the integrated intensities of the fitted CO and CO_2 peaks. The grey bar shows the length of the CO pulse. The CO pulse is positioned at the time of the shift to higher apparent binding energy of the O_2 doublet. The use of the O_2 doublet shift to position the CO pulse will be used later in the surface spectra.

The first observation to make from figure 15 a), b) and c) is that the CO_2 production rapidly ceases when the O_2 peaks shift to higher apparent binding energies. This is consistent with the observation from the previous figure, 14. Secondly, the change from active to inactive is slower ($\sim$ 0.8 s) than the change from inactive to active (most of which takes place in $\sim$ 0.4 s).

The conclusions from the gas phase spectra can be summarised as: 1) CO conversion is complete for the first few pulses and becomes partial for the remainder of the pulse train, 2) during partial CO conversion each pulse has complete CO conversion in the beginning of the pulse and none at the end, 3) the surface undergoes a slow work function shift during the course of pulse train, 4) the work function also changes rapidly when the surface goes between the active and inac-

tive phases, 5) CO in the gas phase is correlated with higher apparent binding energy of the gas phase peaks and 6) the work function shift of the de-activation is slower than for the re-activation.

APXPS surface spectra of FeO/Pt(111):

From the gas phase measurements we learned that loss of CO_2 production is related to a surface change on the sample. In this section we take a closer look at this change by recording surface spectra of FeO_2/Pt(111) during CO oxidation. This is done by moving the sample to the normal measurement position, closer to the analyser (see figure 10). Similarly to the gas phase spectra the image plots were recorded with a repetition rate of 8.5 Hz and binned four times.

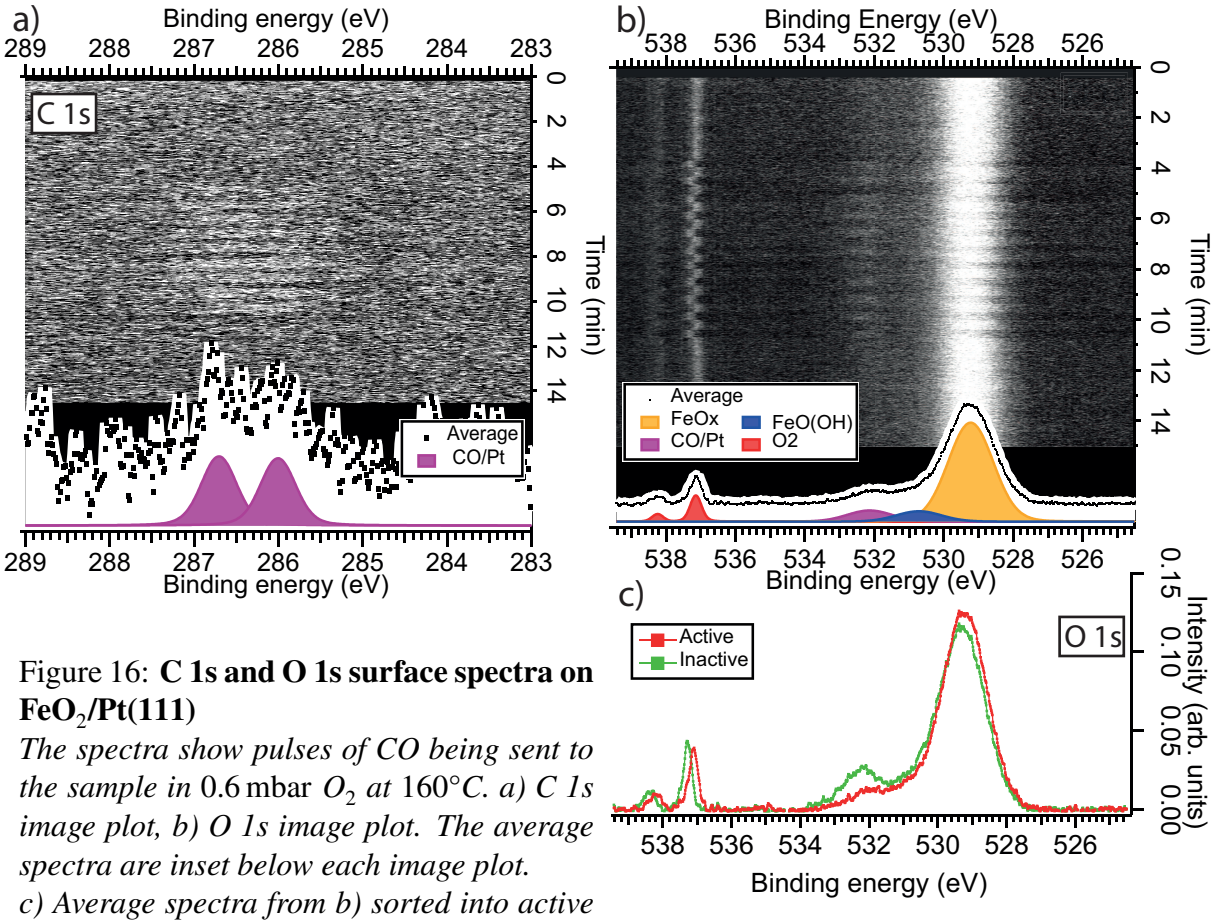

Figure 16: **C 1s and O 1s surface spectra on FeO_2/Pt(111)**
The spectra show pulses of CO being sent to the sample in 0.6 mbar O_2 *at* 160°C. *a) C 1s image plot, b) O 1s image plot. The average spectra are inset below each image plot.*
c) Average spectra from b) sorted into active and inactive phases respectively.

Figure 16 show image plots of C 1s (a) and O 1s (b) acquired during one pulse train for Pt(111) covered with one mono layer FeO_x. The average spectra are inset in bottom of the image plots.

In c) O 1s average spectra of the active (red) and the inactive (green) phases are shown.
In 16 a) the two peaks at ~286.0 eV and ~286.7 eV are attributed to CO adsorbed on a Pt(111) surface (reference from Björneholm[26], who found binding energies of 286.0 eV and 286.7 eV for bridge and atop sites respectively). In 16 b) the doublet at 537-538 eV is attributed to O_2 in the gas phase (like in 13). O_2 is the only gas phase peak that is still visible in the surface spectra due to the light on the sample being 15 times less intense in the surface spectra. The cluster of peaks around ~529 eV is attributed to oxygen in the FeO_2 overlayer with the ~531 eV peak especially attributed to hydroxylysed FeO_2 (from Johansson *et al.* 528.5-531.0 eV[15]). The peak at ~532.2 eV is attributed to CO on a Pt(111) surface (from Björneholm who found 532.7 eV[26]).

The first thing to note in figure 16 a) is that the signal for CO adsorbed on Pt(111) is present in the FeO_x covered sample. The coverage of FeO on the Pt sample in 16 was checked by dosing it with CO just after the film was grown and it was found that no CO was adsorbed and that the coverage was therefore above 1 ML. The fact that we now observe the fingerprint of CO adsorbed on Pt(111) means that the coverage has decreased since the film was checked. This is interesting since Sun *et al.* reported that the FeO/Pt(111) film is stable during CO oxidation at 6 mbar total pressure with a 1:2 CO:O_2 ratio at 450 K[10], conditions quite similar to the ones used in our experiment. Sun *et al.* found that at higher partial pressures of CO the film dewetts and exposes the Pt(111). This is most likely what has happened. The CO:O_2 ratio in our experiment was oxygen rich in that it contained more oxygen than needed to convert all the CO to CO_2 and still the film dewetted. This shows that the CO interacts with the oxide layer even when oxygen is available from the gas phase.
The CO signal from figure 16 offers us an explanation to the lost CO_2 production as it is consistent with CO poisoning, a well-known and well-studied phenomenon for Pt (for example by Langmuir[27], who exlained the phenomenon, Dhar[28] or Camara[29]). Therefore we conclude that CO oxidation takes place at the bare Pt(111) patches formed between FeO islands.

Wadayama *et al.* report that an Fe ML on Pt(111) reconstructs by Fe diffusing into the subsurface layers to form an alloy, if deposited at 470 K[30]. Jerdev *et al.* found that Fe films deposited on Pt(111) and annealed at temperatures between 330-600 K create a surface alloy of Fe and Pt, formed by surface migration of Pt.[31] This surface alloy is stable up to temperatures of 950 K before Fe segregates deeply into the Pt bulk. If, in our experiment, the FeO_2 film is reduced to the degree that bare Fe is left on the Pt(111) surface, for example on FeO-Pt(111) boundaries, it is possible that it segregates into the near surface region of the platinum. Even if the rate of segregation of the Fe atoms would be slow, it could explain the (slow) decrease in surface Fe observed in our experiments. Also, the activity of such an alloy must be considered, if it is formed. Igarashi *et al.* report that Pt alloyed with as little as 5% Fe shows a higher tolerance towards CO poisoning during H_2 oxidation than pure Pt.[32] In Igarashi's experiments Fe was not present on the Pt-Fe alloy surface.

Turning to the O 1s image in figure 16 b) it can be seen that CO is periodically adsorbed on the Pt(111) surface, a result that is consistent with the C 1s image in a). Any peak from oxygen adsorbed on Pt(111) cannot be distinguished in the spectra as it overlaps with the FeO_x peaks. This issue will be treated later in the section for the reference spectra on bare Pt(111).
In figure 16 b) it can be seen that the O_2 doublet shifts binding energies during the pulse train, like in figure 13 b), indicating the same work function shift as in the O 1s gas phase figure. The CO/Pt(111) signal can also be seen to correlate with the O_2 doublet shift. In the oxygen ambience before the pulse train is sent to the sample the Pt(111) patches are most likely covered by oxygen and the rapid work function changes in figure 16 b) are therefore attributed to the replacement of O by CO on bare Pt(111) patches. As the O_2 shift is correlated with CO in the gas phase we can now also conclude that CO adsorbed on Pt(111) is correlated with CO in the gas phase.

The difference between FeO and FeO_2 was discussed in figure 9 where it was found that FeO is characterised by a peak at 529.4 eV and that FeO_2 has three components at $\sim$ 529 eV and a shoulder at 530.6 eV. In figure 16 b) the stronger component can be seen at $\sim$529 eV and a shoulder at $\sim$531 eV, indicating presence of FeO_2. However, FeO could also be present and the exact composition is for now unknown. We note that O/Pt(111) has binding energies that are very close to FeO and FeO_2 on Pt(111) and that also O/Pt(111) could be present in the FeO/Pt(111) spectrum in b).
As discussed, CO adsorbs on the bare Pt(111) patches but to obtain more information about what happens on the FeO/Pt(111) surface the FeO peaks have to be analysed. In 16 b) it can be seen that the intensity of the FeO peaks decrease periodically during the pulse train and that this decrease seems to be correlated with the work function change. One has to keep in mind that the gas composition over the sample changes and that the mean free path of the electrons thereby changes. Therefore, it is difficult to say whether the intensity oscillation is due to changes on the surface or changes in the gas (or both). The average spectra in figure 16 c) indicate a change in the FeO overlayer and such a shift could tell whether the composition of the FeO_x film changes during the reactions, for example between FeO_2 and FeO. A tentative mechanism that can explain the removal of O from the FeO overlayer is the reduction of FeO_2 to FeO either by reaction with CO directly or by spill-over from the oxide to the bare Pt(111) patches, where it reacts with CO and leaves as CO_2.

To conclude, figure 16 gives clear evidence that there must be bare Pt(111) patches on the FeO/Pt(111) sample and that CO adsorbs there. However, CO does not stay on the FeO/Pt(111) during the entire pulse train but is only periodically adsorbed. CO adsorption on Pt(111) was also found to be correlated with higher apparent binding energy of the O_2 doublet. Figure 16 b) and c) indicate that the FeO overlayer changes during the pulse train.

To get a clearer picture of this change the binding energy and intensity of the FeO component from figure 16 b) are shown in figure 17, together with the binding energy of the strongest O_2 component and the intensity of the FeO(OH) component. Figure 17 shows binned versions of the binding energies and intensities. The binning was done by using the O_2 doublet apparent binding energy shift as criterion, as it signals the change between active and inactive states of the sample. The spectra in between two switching events were divided in three with one bin each. This results in spectra that average the first third, middle third and last third of each surface state before it switches again. This makes it possible to track changes in the surface from one pulse to the next as well as seeing changes during a pulse. The fitted binding energies of the strongest O_2 component and the FeO_x peak are plotted in figure 17 a), note the different binding energy scales for the two components. In figure 17 b) the fitted intensities of the FeO_x and FeO(OH) components are shown. The duration of the CO pulses (marked with grey bars) are based on figure 15 where CO + CO_2 intensity is approximated to maximised at the time of the O_2 doublet shift to higher binding energies.

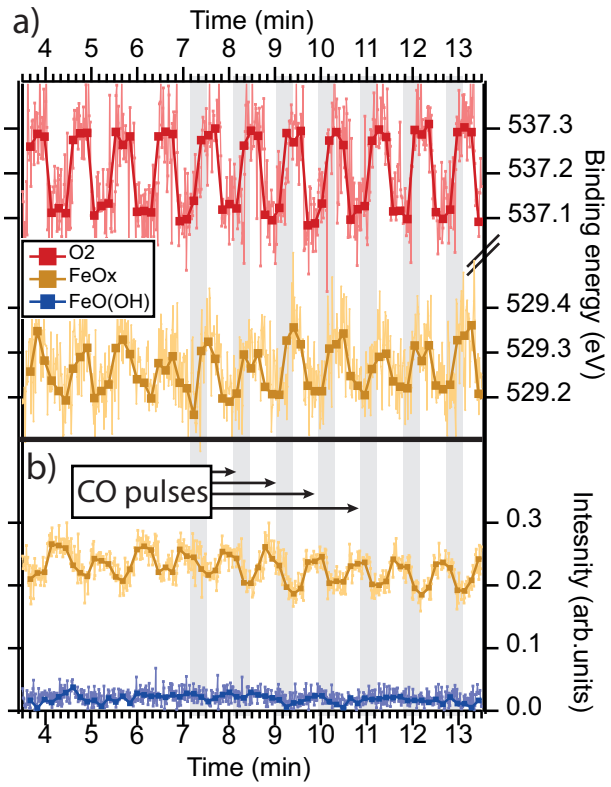

Figure 17:
O 1s surface spectra binned using the O_2 shift
The images show pulses of CO being sent to the sample at 0.6 mbar *at* 160°C. *Panel a) shows the fitted binding energies for FeO_x and O_2 for each spectrum in 16 b). Note the different binding energy scales for O_2 and FeO. b) shows the fitted intensities for the FeO_x and FeO(OH) components. The grey bars are the approximated duration of the CO pulses, based on figure 15.*

It is seen in the apparent O_2 binding energy in figure 17 a) that the surface changes quickly from one state to another and that the work function stays relatively constant until the next switching event, as already seen in figure 15. The FeO_x component also shifts in binding energy and intensity when the O_2 doublet does, although both the binding energy and the intensity fluctuate much more during a pulse for FeO_x. While the FeO_x component is affected by the work function change of the sample, the FeO(OH) component is not: it does not change in binding energy (not shown) or intensity in correlation with the work function shift. This shows that the number of hydroxyl groups in the FeO overlayer is unaffected by the CO oxidation.

It can be seen that in the beginning of a CO pulse the intensity of the FeO peak shifts to lower values while the binding energy shifts to higher values. This is consistent with a change from an overlayer with more FeO_2 to one with less FeO_2 and more FeO. Together with the slower work function changes seen in figure 13 b) an image emerges of an FeO_2 overlayer that is slowly reduced to a mix of FeO_2 and FeO during CO oxidation with quicker changes when CO adsorbs or desorbs from the Pt(111) patches. It appears that the FeO_x overlayer is reduced during the pulses and is recovering during the breaks. The CO/Pt(111) signal is stronger when the FeO film is more reduced, as seen in figure 16 c). If the recovery of the reduced FeO film is dependent on O_2 being adsorbed on the bare Pt(111) patches this could explain why the FeO film does not recover until the adsorbed CO is gone.
To get even more detailed information about how the FeO_x changes during a pulse several spectra can be added together in the same way that was done in figure 15. These images are shown in figure 18 and will be treated next.

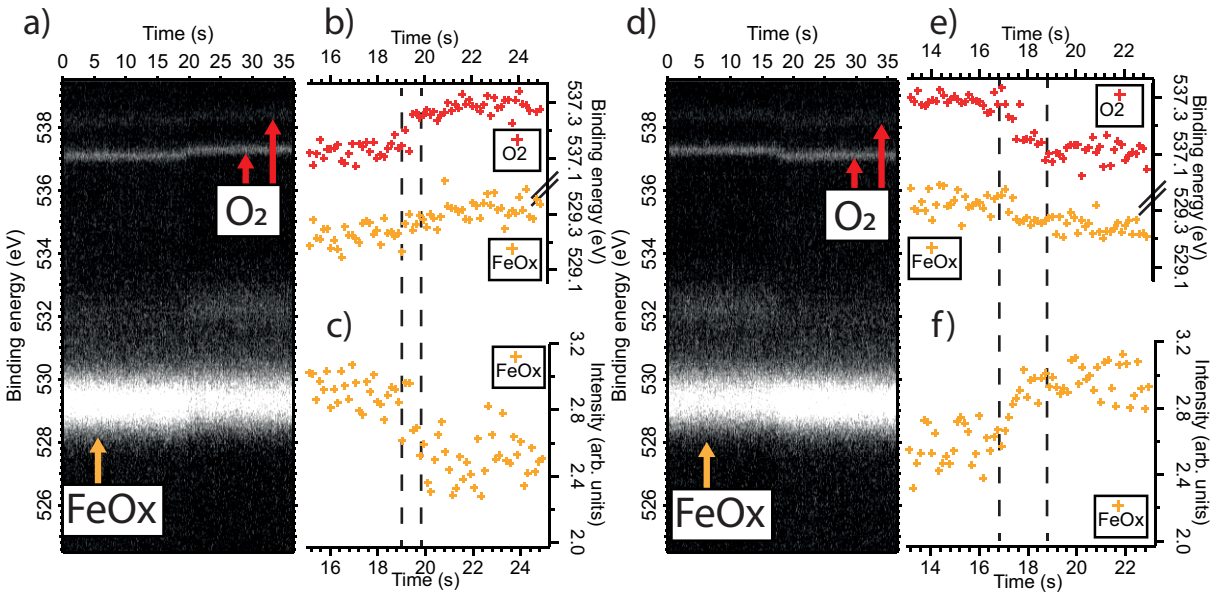

Figure 18: **O 1s surface spectra during the O_2 shift**
The images show pulses of CO being sent to the sample at 0.6 mbar *at* 160°*C. a) and d) show combined images from 11 pulses aligned so that a) the O_2 binding energy falls coincide and b) the O_2 binding energy rises coincide. b) and e) show the binding energy of the strongest O_2 component and the FeO_x component for each case. c) and f) show the intensity of the FeO_x component for each case.*

The image from figure 16 b) has been used to add and align spectra from the last 11 pulses and are shown in figure 18. Panel a) and d) show the resulting image plots averaged over the change from active to inactive phase (a) and from inactive to active phase (b), respectively. The images are not binned in time and have a displayed repetition rate of 8.5 Hz. Panel b) and e) show the

fitted apparent binding energy of the strongest O_2 component and the FeO_x peak for the two cases. Panel c) and d) show the integrated intensity of the fitted FeO_x peak for the two cases respectively.

Looking at when the O_2 doublet shifts to higher binding energies in figure 18 a), b) and c) it can be seen that this shift is faster than the shift to lower apparent binding energies in d), e) and f), the shifts are marked with dashed lines. This is consistent with the observation from the corresponding gas phase image in 15. In the previous section it was speculated that the FeO overlayer undergoes a rapid change when the CO arrives to the sample and the graphs in figure 18 a), b) and c) confirms this. The FeO_x component shifts to lower intensity and higher binding energy just when the O_2 doublet shifts to higher binding energies. As discussed before, the O_2 doublet shifts when the CO_2 intensity is at its maximum and the shift is correlated with CO in the gas phase and CO adsorption on the bare Pt(111) patches. Some details to note is that the intensity shift of the FeO_x component is relatively fast and does not appear to continue after the O_2 doublet has shifted, even though figure 15 indicates that CO should still be present for some time over the sample. Part of this could be explained by loss of O/Pt(111) from the bare Pt(111) patches, whose peak overlaps with the FeO_x components and should be present in the active phase. The shift in binding energy of the FeO_x component is slower and more gradual. This means that the FeO_x film would not start to recover oxygen until the O_2 doublet is shifted back. As the shifting of the O_2 doublet to higher apparent binding energy was identified with CO adsorption on Pt(111) in the analysis of figure 16 this would mean that the film does not recover while CO is adsorbed on the Pt(111) patches, at least not quickly. It is known that the trilayer FeO_2 film can be grown from bilayer FeO and O_2 from the gas phase as this was done when the FeO_2 film was grown before the CO pulses were sent. A possible explanation for the FeO_x overlayer recovery only when O_2 adsorbs on bare Pt(111) is that the O/Pt(111) speeds up the oxidation of the FeO film.

The gas phase and surface can be summarised as: 1) CO conversion is complete for the first few pulses and partial for the remaining pulses, 2) The partially converted CO pulses are a result of each pulse having an initial conversion rate of 100% which drops to 0% at some point during the pulse, 3) the surface undergoes a slow work function shift during the course of pulse train, 4) the work function changes rapidly when the surface goes between the active and inactive phases, 5) the de-activation is slower than the re-activation, 6) the surface spectra showed that there must be bare Pt(111) patches on the FeO/Pt(111) sample and that CO adsorbs there, 7) CO only adsorbs periodically on the Pt(111) during the pulse train and 8) the transition from active to inactive phase is accompanied by a shift of the FeO_x components to higher binding energies and slightly lower intensity, indicative of a loss of surface oxygen in the FeO_2 film.

APXPS gas phase spectra of clean Pt(111):

To check the results obtained for the FeO_x/Pt(111) sample in the previous section the same measurements were done on a clean Pt(111) surface. Like in the FeO/Pt spectra in figure 13, the gas phase O 1s image and average spectra are in log scale and all spectra were recorded with a repetition rate of 8.5 Hz and have been binned four times. Both gas phase image plots are also recorded with the sample retracted 0.3 mm from the normal measurement position.

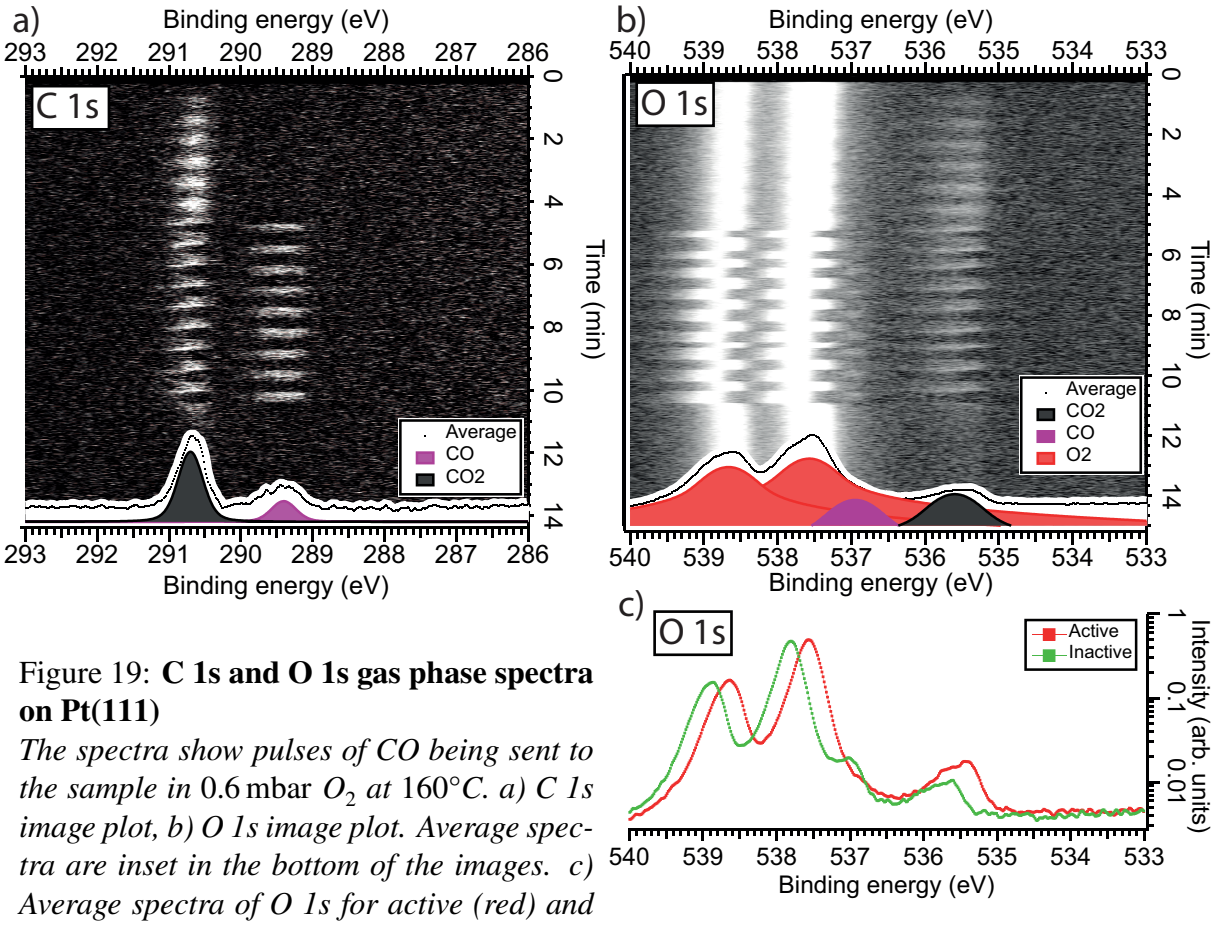

Figure 19: **C 1s and O 1s gas phase spectra on Pt(111)**
The spectra show pulses of CO being sent to the sample in 0.6 mbar O_2 *at* 160°C. *a) C 1s image plot, b) O 1s image plot. Average spectra are inset in the bottom of the images. c) Average spectra of O 1s for active (red) and inactive (green) phase respectively.*

Figure 19 is the reference spectrum for figures 12 and 13. Figure 19 a) and b) show image plots of C 1s and O 1s respectively acquired during one pulse train for a clean Pt(111) crystal at 160°C. The summed spectra from the APXPS image plots are inset at the bottom of each panel. In c) the O 1s average spectra of the active (red) and inactive (green) states are shown.

In figure 19 a) the peak at ~ 291 eV is attributed to gas phase CO_2 and the peak seen at ~ 289.5 eV is attributed to gas phase CO. In b) the two strong shifting peaks at ~ 538 eV and ~ 539 eV are both attributed to the O_2 doublet, while the peak at ~ 536 eV is attributed to gas phase CO_2 and the weak peak at ~ 537 eV is attributed to CO.

The first observation to be made is that the behaviour of the Pt(111) surface is qualitatively very similar to the FeO/Pt(111) surface in figures 12 and 13. Both samples show complete conversion of the first few pulses while subsequent pulses are only partially converted. Also the periodic work function shift is reproduced in the Pt(111) spectra. The work function shift when going between the active and inactive phases is larger on the Pt(111) sample: it is 0.25 eV (compared with 0.11 eV for the FeO_xPt(111) sample). Smaller oscillations in the work function can also be seen in the early part of the pulse train when CO is completely converted to CO_2.

Compared in figure 20 are the average gas phase O 1s spectra for FeO_x/Pt(111) and Pt(111) respectively. FeO_2/Pt(111) spectra are in red above and Pt(111) spectra are in blue below.
From figure 20 it is seen clearly that the work function shifts of the samples are different, the shifts are marked with black lines. In the Pt(111) sample this shift is caused by the CO poisoning and is ~ 0.25 eV. As the FeO_x/Pt(111) also gets CO poisoned the shift seen in the FeO_x/Pt(111) sample could be caused by the same effect but the shift (~ 0.11 eV) being smaller due to a smaller amount of exposed Pt(111).

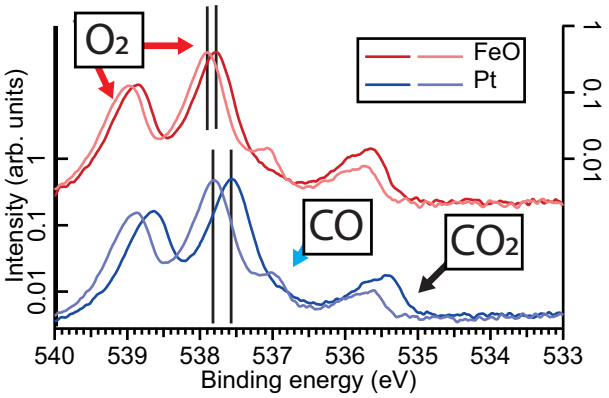

Figure 20: **O 1s gas phase spectra from FeO/Pt(111) and Pt(111)**
Average spectra from figures 12 and 19 c).

For Pt(111) a work function shift of 0.25 eV would mean that the CO poisoned surface would have 0.25 eV lower binding energy than the O covered Pt(111). Collins *et al.*[33] found for a Pt film (assumed predominantly (111)) that the work function shift for CO/Pt was max ~ 0.3 eV while for O/Pt it was max ~ 0.5 eV, both at 295 K. This would fit roughly with our shift of ~ 0.25 eV. On the other hand, work function shifts depend heavily on coverage (and by extension on temperature and pressure) and the references found for work function shifts can vary considerably. For example Wandelt found a work function increase of 0.2 eV for O_2/Pt(111) compared with clean Pt(111) at 170 K and 0.8 eV for a saturated surface at lower temperatures.[34]. Thus, exact predictions are difficult to make unless references exist at the precise temperatures and pressures of interest.

The gas phase spectra from Pt(111) showed a similar behaviour to the FeO_xPt(111) spectra previously seen. The difference in work function between the active and inactive phases is about twice as large on the clean Pt(111) compared to FeO_x/Pt(111). The work function shift found on clean Pt(111) is consistent with a change from an O covered to a CO covered Pt(111) surface .

APXPS surface spectra of clean Pt(111):

In the gas phase spectra from the clean Pt(111) surface it was seen that the behaviour was very similar to that observed on FeO_2/Pt(111) sample. The spectra of the Pt(111) surface are investigated in this section to explain why. Like previous spectra they were recorded with a repetition rate of 8.5 Hz and binned four times.

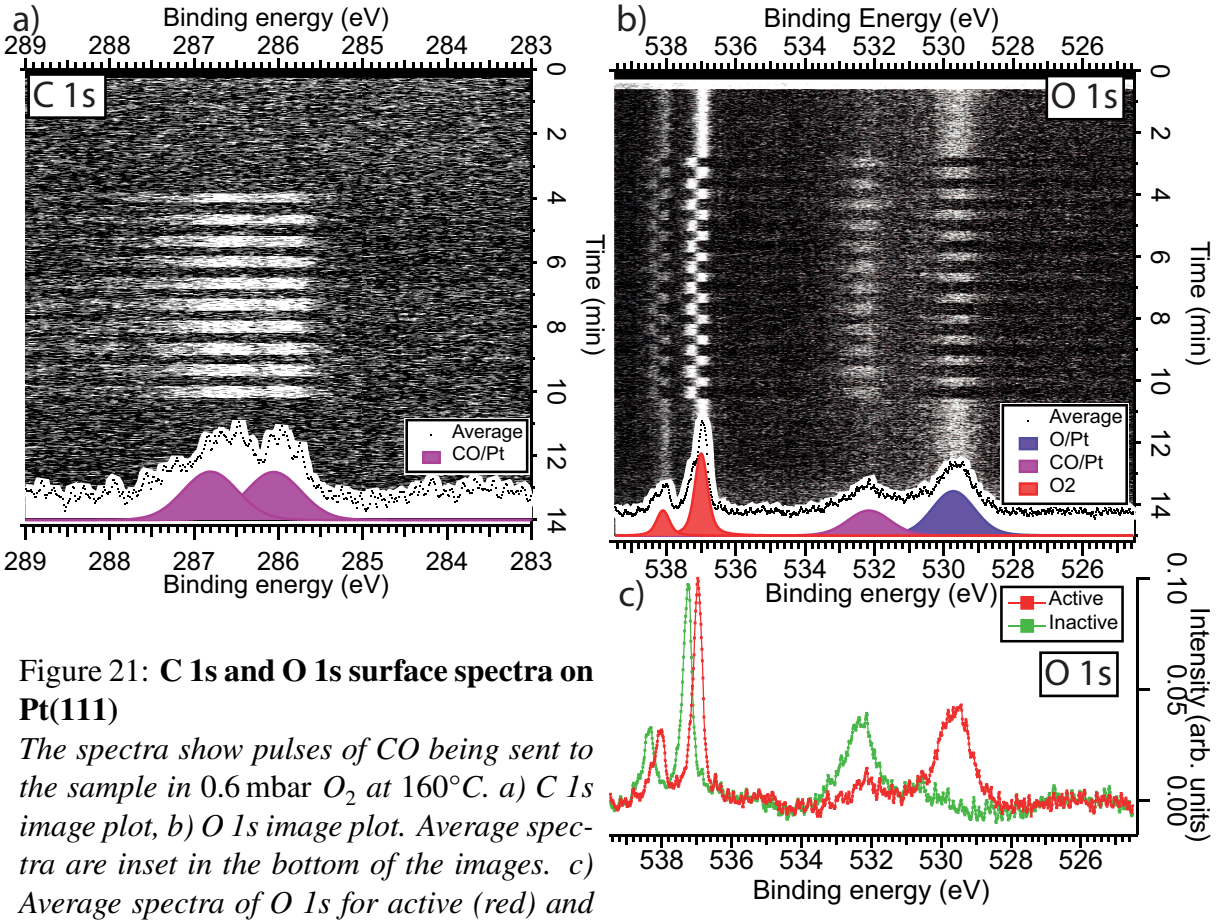

Figure 21: **C 1s and O 1s surface spectra on Pt(111)**
The spectra show pulses of CO being sent to the sample in 0.6 mbar O_2 *at* 160°*C. a) C 1s image plot, b) O 1s image plot. Average spectra are inset in the bottom of the images. c) Average spectra of O 1s for active (red) and inactive (green) phase respectively.*

Figure 21 a) and b) show image plots from C 1s and O 1s respectively acquired during one pulse train for clean Pt(111) and is the reference spectra of figure 16. The average spectra for each

image plot are inset at the bottom. In c) the two average spectra of O 1s for the active (red) and inactive (green) phases are shown.

The two peaks at ~286.0 eV and ~286.7 eV in 21 a) are attributed to CO adsorbed on a Pt(111) surface (compare with Björneholm[26], who found binding energies of 286.0 eV and 286.7 eV). In 21 b) the doublet at 537-538 eV is attributed to O_2 in the gas phase. The peak at ~532.2 eV is attributed to CO on a Pt(111) surface (from Björneholm who found 532.7 eV[26]) and the peak at ~529.6 eV to O chemisorbed on Pt(111) (Puglia *et al.*, 529.83 eV[35]).

CO adsorbs very readily on the Pt(111) surface, as seen in 21 a). The CO/Pt(111) signal from figure 21 confirms the explanation to the lost CO_2 production seen previously in figure 19, that it is caused by CO poisoning of Pt(111). The clean Pt(111) surface does not stay poisoned for the whole pulse train, it is only poisoned periodically. Looking more closely at the O1s spectra in 21 b) the signatures of chemisorbed O and CO adsorbed on Pt(111) can be seen to be mutually exclusive of each other. The Pt sample starts by being covered with oxygen, which is eventually replaced by CO when a pulse is passing over the sample. It was seen in the previous figure, 19, that the first pulses are completely converted and only 10 CO poisoned periods can be seen in figure 21 a) (12 periods in 21 b)), it takes a while for the surface to start becoming poisoned. This is consistent with the model of an oxygen covered Pt catalyst converting CO to CO_2, which is then periodically poisoned and ceases to convert CO. The shift in O_2 doublet binding energy in 21 b) also correlates with the change between an O and a CO covered Pt(111) surface. The shift can be understood as a consequence of a work function change of the sample when O is replaced by CO on the surface, or vice versa.
Further, we can identify lower binding energies of the O_2 doublet with an oxygen covered Pt(111) surface and higher binding energies with a CO covered surface.

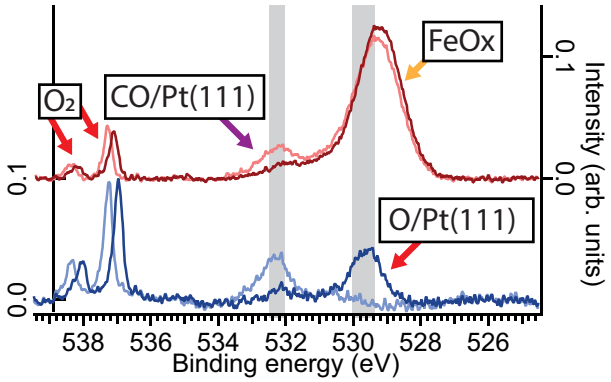

Figure 22: **O 1s surface spectra from FeO/Pt(111) and Pt(111)**
Average spectra from figures 16 c) and 21 c). The grey bars mark the positions of the CO/Pt(111) and O/Pt(111) peaks respectively.

As it was seen in the FeO_x/Pt(111) spectra in figure 16 that also the FeO_x/Pt(111) sample is affected by CO poisoning it is necessary to compare the FeO/Pt(111) and Pt(111) spectra more closely. This is to exclude that the shift seen in the FeO_x peak in the analysis of the FeO_x/Pt(111) O 1s spectra comes from events at the exposed Pt(111) patches. Figure 22 shows the O 1s average spectra for the active and inactive phases from figures 16 c) and 21 c) respectively. FeO_2/Pt(111) spectra are in red above and Pt(111) spectra are in blue below.

Looking at the surface spectra in 22 it can be seen that the peak positions in the FeO_x/Pt(111) and clean Pt(111) overlap well for the CO poisoned state (lighter colours). In the bare Pt(111) spectrum the O/Pt(111) peak can be seen clearly in the non-poisoned state (darker blue). As the FeO_x sample has patches of bare Pt(111) due to dewetting an O/Pt(111) should be present also in its spectra, but it is not distinguishable from the FeO_x peaks. An O/Pt(111) peak in the FeO_x/Pt(111) spectrum should contribute to the intensity of the peaks in the FeO_x region and an intensity increase be seen. In the active state of FeO_x/Pt(111) there is an intensity increase at ~ 528-529 eV but the O/Pt(111) peak is centred around 529.8 eV. This can mean two things, either that the shift in the FeO_x region is caused by changes in the FeO_x film or the binding energy of the chemisorbed O on Pt(111) is shifted to lower values due to interaction the FeO overlayer. It should be remembered that the bilayer FeO peak (I) is at 529.4 eV and practically coincides with the O/Pt(111) peak. CO poisoning of the Pt(111) patches would cause an intensity decrease at ~529.8 eV while if the FeO_x overlayer changes from originally a predominantly FeO_2 trilayer film to a more FeO bilayer structure when poisoned an intensity increase would be expected at ~529.4 eV. For the FeO_x/Pt(111) sample a decrease in the O/Pt(111) peak could be accompanied by an intensity increase in the FeO (I) peak, resulting in little change in the region 529-530 eV. To determine which of these scenarios is most likely is difficult, but a shift of ~1 eV of the O/Pt(111) peak due to the presence of the oxide layer would be a large shift.

To try to quantify the change in the overlayer asymmetric peaks were used (like the characterisation in figure 9) to fit O 1s peaks to the FeO_x components from figure 16 c). The result is displayed in figure 23. The binding energy of O/Pt(111) and FeO (I) are too close to fit separately and they are represented by the same peak in figure 23. The relative change in intensity when going from active to inactive phase are (I) + O/Pt(111): ~ 1.38, (III): ~ 0.80, (IV): ~ 0.63 and CO/Pt(111): 2.36. In words, when going from active to inactive phase the intensity decreases for the FeO_2/Pt(111) components (III) and (IV) and increases for the FeO bilayer (I) and O/Pt(111) peaks. This observation supports the hypothesis that the CO oxidation reaction uses oxygen from the FeO_2 trilayer film and transforms some of it into bilayer FeO. The (II) component was not possible to fit accurately and has been omitted and a peak for CO/Pt(111) was added.

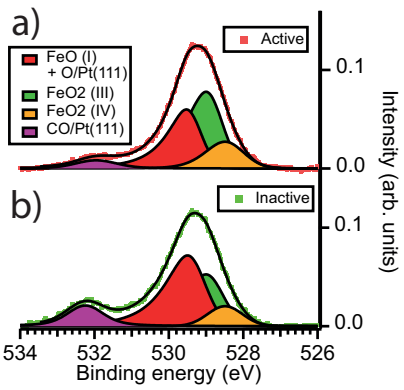

Figure 23: **O1s fits**
Fitted peaks to the FeO_x overlayer in the active (a) and inactive (b) phase.

In summary the Pt(111) reference spectra showed that CO poisoning is the process that determines the activity of both the FeO_x/Pt(111) and Pt(111) samples. The work function observed when the samples change between active and inactive states is caused by CO and O adsorption on the bare Pt(111) areas of the sample. While the XPS spectra show little difference between the two samples we turn to the other technique used in this work, QMS, to check the result.

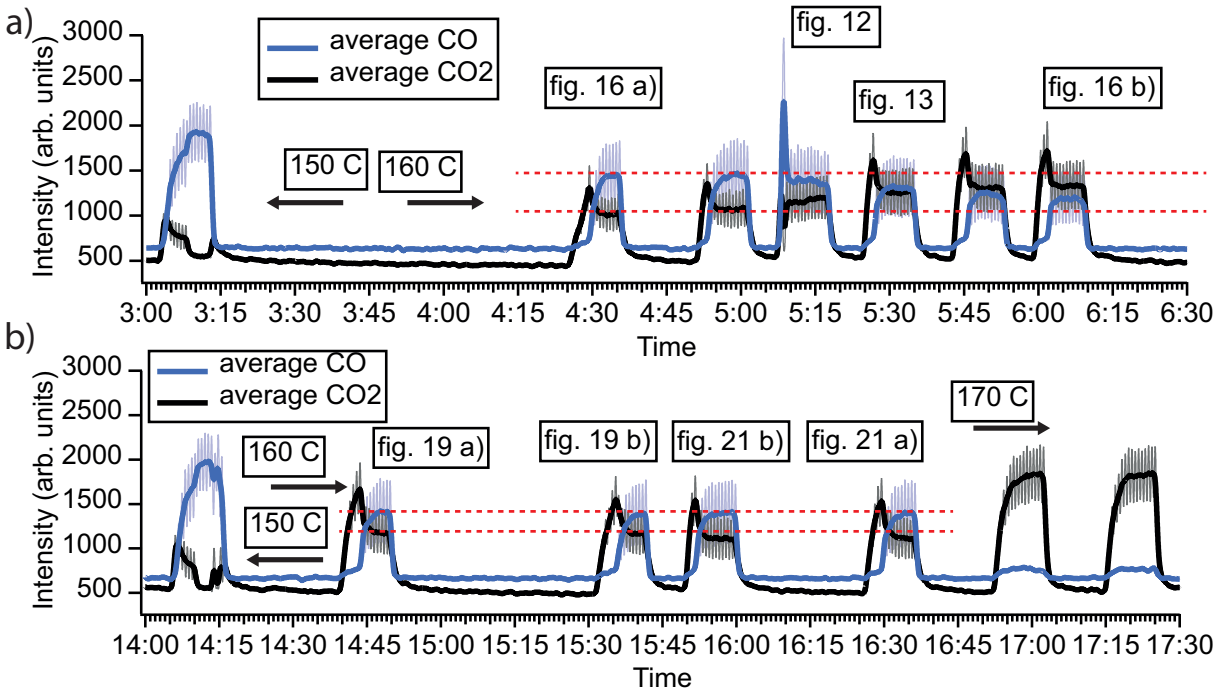

Figure 24: **QMS signal of CO and CO_2 at** 160°**C**
The average CO and CO_2 presence during CO pulses at 160°*C over the FeO/Pt(111) sample (a) and clean Pt(111) sample (b). The red lines mark the maximum CO and CO_2 levels for the first pulse train.*

In figure 24 the average CO and CO_2 concentration during the pulse trains at 160°C is shown for FeO_x/Pt(111) (a) and bare Pt(111) (b). The gas was probed just above the sample by sampling the gas through the aperture positioned approximately 600 µm above the surface. The plots contain one pulse train at 150°C for reference and then 4-6 pulse trains at 160°C. The Pt(111) plot contains two pulse trains at 170°C. Individual pulses are indicated by faint lines while average concentration is shown with thicker, darker lines. The pulse trains are marked with the number of the figure that contains the corresponding XPS spectrum of that pulse train.

At first glance the samples behave identically, the first pulses are completely converted to CO_2 and the subsequent pulses are only partially converted (regions with co-existence of CO_2 and CO in figure 24), the same result as seen in the XPS spectra above. Looking at the pulse trains

on clean Pt(111) (24 b)) at 160°C the maximum produced CO_2 is the same for all pulse trains, as indicated by the dashed red lines. This is not the case for the FeO_x/Pt(111) sample. In 24 a) the lower red dashed line indicate the original maximum CO_2 production and it can be seen that the conversion rate increases for every pulse train that is sent to the sample. The first pulse train (marked "figure 16 a)") that is sent to the FeO sample at 160°C has lower while the last pulse train (marked "figure 16 b)") has higher CO conversion ratio than the pure Pt(111)at the same temperature. This shows that while the behaviour of the two samples looks similar the FeO/Pt(111) is in fact the more active catalyst, it just does not reach the more active state immediately. The activity of the FeO/Pt(111) sample could be increasing just due to being at elevated temperatures for long enough or it could be caused by the reaction itself. A closer look at the "figure 12" pulse train at ~ 5:15 in 24 a) gives a hint. It is the same pulse train as already seen by APXPS in figure 12 with the pure unconverted CO pulse in the beginning of the pulse train. The reason for the failure of the sample to convert this pulse is still unknown, but it can be seen in figure 24 a) that the activity of the sample increases more rapidly in that pulse train. This indicates that the activity of the FeO_x sample increases in reducing conditions, such as a high CO concentration.

As the FeO film is known to dewett and expose bare Pt(111) during CO oxidation one possible scenario explaining the increased activity is that the dewetting exposes more active Pt(111). However, since the activity of the FeO_x sample is higher than for bare Pt(111) by the time of the last pulse train this explanation is not satisfactory. This assumes, of course, that the temperature was the same on both samples. As it is deemed unlikely that the temperature of the two samples would be different when the observed behaviour is so similar at temperatures below 150°C and for the first pulse trains at 160°C the temperatures of the FeO_x/Pt(111) and Pt(111) samples in figure 24 are deemed to be similar enough.

When the FeO overlayer dewetts it does not only expose more Pt(111) to the gas, it also exposes more FeO-Pt(111) boundaries to the gas. Therefore it is possible that the increased activity is caused not only by increased Pt(111) exposure but also by increased density of FeO edge sites. Fu *et al.* proposed that the increased CO oxidation activity of the FeO/Pt(111) sample was caused by exposed iron atoms on the FeO-Pt(111) boundaries [11] and our observation of gradually increasing activity and dewetting for a 1ML FeO_2/Pt(111) would support this hypothesis. However, as seen in figures 17 and 18 the FeO_2 overlayer also goes through changes during reactions and its role in the activity cannot be distinguished from that of the FeO-Pt(111) boundaries.

The analysis of the QMS data confirms that the FeO_x/Pt(111) sample is in fact more active than bare Pt(111), although it is not immediately apparent when looking only at the APXPS spectra. The activity of the FeO_x/Pt(111) sample increases with time and is proposed to be driven by the CO oxidation reaction. How the activity is increased is still unclear.

QMS data from the first beam time

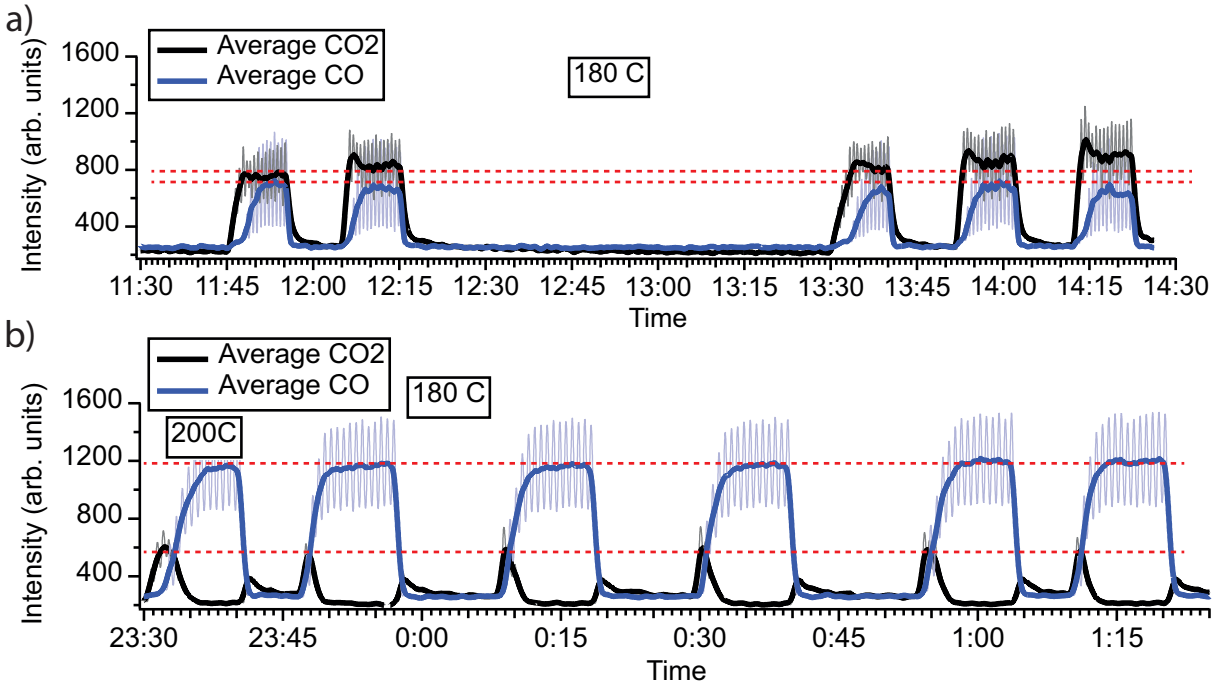

Figure 25: **QMS signal of CO and CO_2 from the first beam time**
The average CO and CO_2 presence during CO pulses at 180°C over the FeO/Pt(111) sample (a) and clean Pt(111) sample (b) from the first beam time. The red lines mark the maximum CO and CO_2 levels for the first pulse train.

The old data, that showed much higher activity for the FeO_x/Pt(111) sample, is shown for reference in figure 25. The gas was probed in the same way as in figure 24. All pulse trains in 25 were sent with the samples first at 200°C and then at 180°C, otherwise the measurements were equal in all respects. The discrepancy in result is speculated to be due to inaccurately measured temperature in this first measurement session. Like before individual pulses are indicated by faint lines while average concentrations are shown with thicker, darker lines.

Qualitatively, the behaviour of the Pt(111) in the old data in figure 25 at 180°C is similar to the behaviour at 140°C in the new data. This is not self-consistent and one of the temperature measurements must be wrong. The FeO_2/Pt(111) sample shows similar or slightly higher activity in the old data (25 a)) at 180°C than in the new data at 160°C, which is more consistent. The conclusion is that the temperature measurement of at least the Pt(111) sample in the first measurement session at 180°C is most likely incorrect.
It can be seen in figure 25 a) that the activity of the FeO_x/Pt(111) sample increases with each pulse train, just like in the other measurement session in figure 24. This behaviour then seems

to be a general and reproducible trend, which is a valuable insight for future experiments.
One difference between the measurements in figure 24 and 25 is that in figure 25 the activity was measured first at 200°C and then at 180°C, stepping down in temperature, while in 24 the temperature was first 140°C, then 150°C and 160°C, stepping up in temperature. As it was observed that the reaction affects the sample in the case for the FeO_x/Pt(111) so will the temperature history of the measurements, as the temperature affects the reaction. Therefore, to get consistent results, it seems like care needs to be taken that the sample is exposed to the same treatment in the same order in the case for the FeO_x/Pt(111) sample.

4 Summary and outlook

In this thesis the oxidation of CO on a FeO_x/Pt(111) and bare Pt(111) surface has been studied. The study showed that the mono layer FeO_x/Pt(111) film dewetts while running the CO oxidation reaction at 160°C and pressures of 0.6 mbar with a CO:O_2 ratio of 1:9. The dewetting exposes bare Pt(111) and FeO-Pt(111) boundary to the gas. The dewetting was found to be a reaction induced process, in agreement with the results from Sun *et al.*.[10] However, our film dewetted at CO:O_2 ratios of at most 1:9 while Sun found that the film only dewetts at ratios of 1:2 CO:O_2 or more CO rich.
Secondly, it was observed that the amount of surface oxygen in the FeO_x trilayer decreases at reaction conditions, indicating a transition to a state more similar to the FeO bilayer. The amount of surface oxygen in the FeO_x trilayer decreases during the course of the pulse train with the fastest and largest losses during the times the Pt(111) patches were CO poisoned.
Finally, we observed that the activity of the FeO_x/Pt(111) sample was initially lower than the Pt(111) reference sample but that after about one hour the activity of the FeO_2/Pt(111) sample had increased to levels higher than the Pt(111) reference. Thus an incubation time was found before the FeO_x/Pt(111) sample reached high catalytic activity reported by many authors.[6;7;8;9;10;11]

As the dewetting exposes FeO-Pt(111) boundaries and the film is composed partially of FeO_2 trilayer it is not possible to attribute the increased activity to one of the proposed models for the low temperature CO oxidation , an active FeO_2 layer proposed by Sun *et al.*[10] or CUF sites at the FeO-Pt(111) boundaries proposed by Fu *et al.*[11] To be able to test the two hypothesises, in future experiments FeO_x/Pt(111) samples should be prepared in such a way that bare Pt(111) is not exposed to the gas. For example FeO/Pt(111) films could be prepared with significantly more than 1 ML coverage to try to prevent dewetting so that the activity of the FeO_2 overlayer could be investigated without the presence of bare Pt(111) of FeO-Pt(111) boundary sites. If the film dewetts, it can be restored by exposure to O_2, as reported by Sun.[10] Whether films that do not dewett under typical APXPS conditions can be made is possible to test without the use of synchrotron light as coverage can be checked by CO adsorption on any exposed Pt(111) with, for example, polarization modulated infrared reflection absorption spectroscopy (PMIRAS) like in

Sun *at al.* or Temperature Programmed Desorption.[10] Films with less than 1 ML coverage could also be prepared to check the role of the FeO-Pt(111) boundaries relative to the bare Pt(111). The FeO_2/Pt(111) sample activity changes in time during CO oxidation and this behaviour should be investigated more thoroughly. A similar set-up could be used to the one used in these experiments with a cone with an aperture close to the sample surface sampling the gas above the sample and analysing its composition with a QMS, but with no synchrotron light as it is not necessary to measure the catalysts net activity. The behaviour of the FeO_2/Pt(111) sample could then be mapped for different CO exposure times at different temperatures to establish if it reaches a steady state. Then the FeO_2/Pt(111) sample could be measured with APXPS at more stable conditions. The degree of dewetting should also be monitored and quantified more often during reactions at any particular temperature. Only the C 1s surface spectra gave a clear indication of the dewetting in our experiments and it was only measured once per temperature interval. If the sample activity would be found to increase with increasing dewetting and reach higher levels than on bare Pt(111) it would be convincing argument that the FeO-Pt(111) boundaries play a critical role for the activity of the FeO/Pt(111) system during CO oxidation.

The FeO/Pt(111) system has also been studied extensively with Scanning Tunnelling Microscopy (STM) (for example in refs[10;22;36]) and this technique could be used to check some of the conclusions and answer some of the questions raised by our study. As the FeO_2, FeO and Pt(111) are easily distinguishable in STM images the change in coverage of each at reaction conditions could be checked. The role of the FeO_2 and FeO in the CO oxidation reaction could then be compared. We also observed that the FeO over layer dewetted at reaction conditions, but we have no information on whether there are any specific sites in the FeO moiré pattern that are more likely to dewett. STM could help answer these questions. As STM gives topographic information the precise time evolution of the sample at reaction conditions could be monitored, providing insights difficult to obtain with XPS.
The electron analyser used during our APXPS experiments does have a spatially resolved mode with 10 µm spatial resolution[19] so if a Pt(111) surface was prepared that is covered with FeO_x in one region and exposing bare Pt(111) in another the difference in activity between the two, as well as the interface between them, could be recorded directly in one shot. This would not give the same resolution that STM provides but allow the high time resolution available in our APXPS set-up as well as the other advantages connected to APXPS as well as removing discrepancies in temperature measurements that can arise when the sample is transferred and cleaned between measurement sessions.
Finally, a question that has not been asked yet in this report is what phase(s) the dewetted film is in. When the film dewetts it crumples into droplets (for example seen in the STM images in Sun's article[10]) where other iron oxide phases could form, besides FeO and FeO_2. For example Fe_2O_3 or Fe_3O_4 regions could form, of which Fe_2O_3 has shown catalytic activity for some hydrocarbons.[37;38]

To conclude, several preparatory experiments could be made to further explore the behaviour of the FeO/Pt(111) system, especially concerning the time evolution of the activity and the FeO overlayer as it is exposed to CO. A more stable FeO_2 sample needs to be found in order to separate the effect of the FeO_2 overlayer and FeO-Pt(111) boundary during reactions, for example with >1 ML coverage. Coverage studies of the FeO/Pt(111) system could help quantify the effect of the FeO-Pt(111) boundaries in CO oxidation on ultra thin iron oxide films. Use of other techniques like PMIRAS and STM could deepen the understanding of the FeO/Pt(111) system and obtain information not possible with XPS.

5 Acknowledgements

I would like to thank Jan Knudsen for good supervision, discussions and feedback during this project. I would also like to thank Tamires Gallo, Giulio D'Accunto, Virgínia Boix and Marie Døvre Strømsheim whom I worked with during the experimental sessions as well as Beam line engineers Suyun Zhu and Andrey Shavorskiy who manage the equipment at the beam line.

References

[1] Recognizing the best in innovation: Breakthrough catalyst. *R&D Magazine*, August 2005. Available at: https://www.rdmag.com/award-winners/2005/08/breakthrough-catalyst, accessed: [10-04-2019].

[2] Vaclav Smil. Detonator of the population explosion. *Nature*, 400, 1999.

[3] J.T. Kummer. Catalysts for automobile emission control. *Progress in Energy and Combustion Science*, 6(2):177 – 199, 1980.

[4] Grigorios C. Koltsakis and Anastasios M. Stamatelos. Catalytic automotive exhaust aftertreatment. *Progress in Energy and Combustion Science*, 23(1):1 – 39, 1997.

[5] S. E. GOLUNSKI. Final analysis. *Platinum Metals Review*, 51(3):162–162, 2007.

[6] Masahiro Watanabe, Yimin Zhu, and Hiroyuki Uchida. Oxidation of co on a pt−fe alloy electrode studied by surface enhanced infrared reflection−absorption spectroscopy. *The Journal of Physical Chemistry B*, 104(8):1762–1768, 2000.

[7] Robin Hirschl, Fran çoise Delbecq, Philippe Sautet, et al. $pt_{80}fe_{20}$ surface from first principles: Electronic structure and adsorption of co and atomic h. *Phys. Rev. B*, 66:155438, Oct 2002.

[8] M. Lewandowski, Y.N. Sun, Z.-H. Qin, et al. Promotional effect of metal encapsulation on reactivity of iron oxide supported pt catalysts. *Applied Catalysis A: General*, 391(1):407 – 410, 2011. Recent Developments in Model Catalysis - Closing the Gap to Technical Applications.

[9] Anna Basińska, Tomasz P. Maniecki, and Wojciech K. Jóźwiak. Catalytic activity in water-gas shift reaction of platinum group metals supported on iron oxides. *Reaction Kinetics and Catalysis Letters*, 89(2):319–324, Aug 2006.

[10] Y.-N. Sun, Z.-H. Qin, M. Lewandowski, et al. Monolayer iron oxide film on platinum promotes low temperature co oxidation. *Journal of Catalysis*, 266(2):359 – 368, 2009.

[11] Qiang Fu, Wei-Xue Li, Yunxi Yao, et al. Interface-confined ferrous centers for catalytic oxidation. *Science*, 328(5982):1141–1144, 2010.

[12] Ying-Na Sun, Livia Giordano, Jacek Goniakowski, et al. The interplay between structure and co oxidation catalysis on metal-supported ultrathin oxide films. *Angewandte Chemie International Edition*, 49(26):4418–4421, 2010.

[13] G.H. Vurens, V. Maurice, M. Salmeron, et al. Growth, structure and chemical properties of feo overlayers on pt(100) and pt(111). *Surface Science*, 268(1):170 – 178, 1992.

[14] G.H. Vurens, M. Salmeron, and G.A. Somorjai. Structure, composition and chemisorption studies of thin ordered iron oxide films on platinum (111). *Surface Science*, 201(1):129 – 144, 1988.

[15] Niclas Johansson, Lindsay R. Merte, Elin Grånäs, et al. Oxidation of ultrathin feo(111) grown on pt(111): Spectroscopic evidence for hydroxylation. *Topics in Catalysis*, 59(5):506–515, Mar 2016.

[16] Livia Giordano, Gianfranco Pacchioni, Claudine Noguera, et al. Identification of active sites in a realistic model of strong metal-support interaction catalysts: The case of platinum (1 1 1)-supported iron oxide film. *ChemCatChem*, 6(1):185 – 190, 2014.

[17] Lindsay R. Merte, Yunhai Bai, Helene Zeuthen, et al. Identification of o-rich structures on platinum(111)-supported ultrathin iron oxide films. *Surface Science*, 652:261 – 268, 2016. Insights into Surface Phenomena: In Honor of John T. Yates Jr.

[18] Elettra, accessed: [22-04-2019].

[19] www.scientaomicron.com, accessed: [15-01-2019].

[20] Dm photonics, accessed: [26-04-2019].

[21] www.wavemetrics.com/, accessed: [23-04-2019].

[22] Jan Knudsen, Lindsay R. Merte, Lars C. Grabow, et al. Reduction of feo/pt(111) thin films by exposure to atomic hydrogen. *Surface Science*, 604(1):11 – 20, 2010.

[23] Weixin Huang and Wolfgang Ranke. Autocatalytic partial reduction of feo(111) and fe3o4(111) films by atomic hydrogen. *Surface Science*, 600(4):793 – 802, 2006.

[24] Luan Nguyen and Franklin (Feng) Tao. Development of a reaction cell for in-situ/operando studies of surface of a catalyst under a reaction condition and during catalysis. *Review of Scientific Instruments*, 87(6):064101, 2016.

[25] Livia Giordano, Gianfranco Pacchioni, Claudine Noguera, et al. Spectroscopic evidences of charge transfer phenomena and stabilization of unusual phases at iron oxide monolayers grown on pt(111). *Topics in Catalysis*, 56(12):1074–1081, Aug 2013.

[26] O. Björneholm, A. Nilsson, H. Tillborg, et al. Overlayer structure from adsorbate and substrate core level binding energy shifts: Co, cch3 and o on pt(111). *Surface Science*, 315(1):L983 – L989, 1994.

[27] Irving Langmuir. The mechanism of the catalytic action of platinum in the reactions 2co + o2= 2co2 and 2h2+ o2= 2h2o. *Trans. Faraday Soc.*, 17:621–654, 1922.

[28] H. P. Dhar, L. G. Christner, and A. K. Kush. Nature of co adsorption during h 2 oxidation in relation to modeling for co poisoning of a fuel cell anode. *Journal of The Electrochemical Society*, 134(12):3021–3026, 1987.

[29] G. A. Camara, E. A. Ticianelli, S. Mukerjee, et al. The co poisoning mechanism of the hydrogen oxidation reaction in proton exchange membrane fuel cells. *Journal of The Electrochemical Society*, 149(6):A748–A753, 2002.

[30] Toshimasa Wadayama, Hiroshi Osano, Toshiaki Maeyama, et al. Infrared reflection absorption study of carbon monoxide adsorption on fe/pt(111) bimetallic surfaces. *The Journal of Physical Chemistry C*, 112(24):8944–8950, 2008.

[31] Dmitri I. Jerdev and Bruce E. Koel. Fe deposition on pt(111): a route to fe-containing pt–fe alloy surfaces. *Surface Science*, 513(1):L391 – L396, 2002.

[32] Hiroshi Igarashi, Takeshi Fujino, Yimin Zhu, et al. Co tolerance of pt alloy electrocatalysts for polymer electrolyte fuel cells and the detoxification mechanism. *Phys. Chem. Chem. Phys.*, 3:306–314, 2001.

[33] Douglas M Collins, James B Lee, and W.E Spicer. A photoemission and thermal desorption study of carbon monoxide and oxygen adsorbed on platinum. *Surface Science*, 55(2):389 – 402, 1976.

[34] K. Wandelt. Photoemission studies of adsorbed oxygen and oxide layers. *Surface Science Reports*, 2(1):1 – 121, 1982.

[35] C. Puglia, A. Nilsson, B. Hernnäs, et al. Physisorbed, chemisorbed and dissociated o2 on pt(111) studied by different core level spectroscopy methods. *Surface Science*, 342(1):119 – 133, 1995.

[36] Wilhelmine Kudernatsch, Guowen Peng, Helene Zeuthen, et al. Direct visualization of catalytically active sites at the feo–pt(111) interface. *ACS Nano*, 9(8):7804–7814, 2015. PMID: 26027877.

[37] W. Weiss, D. Zscherpel, and R. Schlögl. On the nature of the active site for the ethylbenzene dehydrogenation over iron oxide catalysts. *Catalysis Letters*, 52(3):215–220, Jul 1998.

[38] Yvonne Joseph, Mario Wühn, Arno Niklewski, et al. Interaction of ethylbenzene and styrene with iron oxide model catalyst films at low coverages: A nexafs study. *Phys. Chem. Chem. Phys.*, 2:5314–5319, 2000.